Table 1
mRNA expression of Fp isoforms in human cultured cells and tissues.

The expression ratio of the two Fp isoforms was analyzed by RT-PCR-RFLP (restriction fragment length polymorphism with AvaII). Total RNAs were obtained from NIPPON GENE (Japan) for normal liver, heart, skeletal muscle, brain, kidney and breast tumor, colon tumor, stomach tumor and uterus tumor. Wako (Japan) for normal pancreas and fetal tissues. Invitrogen (USA) for normal testes and breast tumor, liver tumor, kidney tumor, colon tumor, pancreas tumor, cervix tumor, ovary tumor, prostate tumor. Cells; Fibroblast and Myoblast: kind gift from Dr. Yu-ichi Goto (National Institute of Neuroscience, Japan) A549, DLD-1 and MCF-7: kind gift from Mr. Yasuyuki Yamazaki (Taiho pharma ceutical, Japan) Panc-1: kind gift from Dr. Yasuhiro Esumi (National Cancer Institute, Japan) Raji: kind gift from Dr. Kazurou Shiomi (Kitasato university, Japan) HT-29, HU-VEC-C, MDA-M-231, BT-20 and T-47D: ATCC (USA). Pancreatic epithelial and stromal cells: DS pharma (Japan).

		Race	Gender	Age	I (%)/II (%)
Tissue (normal)	Liver[*]	Caucasoid	Female	15	70/30
	Heart[*]	Caucasoid	Pool of 7 donors		61/39
	Skeletal muscle[*]	––	Male	23	80/20
	Brain[*]	Caucasoid	Male	50	84/16
	Kidney[*]	Caucasoid	Pool of 8 donors		62/38
	Pancreas	––	Male	44	30/70
	Testes	Caucasoid	Male	19	100/0
Cell (normal)	Fibroblast[*]	Mongoloid	––	––	94/6
	Myoblast[*]	Mongoloid	––	––	87/13
	HUV-EC-C[*]	––	––	––	88/12
	Pancreatic epithelial	––	––	––	100/0
	Pancreatic stromal	––	––	––	100/0
Tissue (fetal)	Brain	––	Female	22 weeks	100/0
	Brain	––	Male	41 weeks	38/62
	Skeletal muscle	––	Male	22 weeks	0/100
	Skeletal muscle	––	Female	19 weeks	100/0
Tissue (cancer)	Breast	––	Female	55	100/0
	Breast	Mongoloid	Female	Pool of 6 donors	0/100
	Liver	Caucasoid	Male	60	0/100
	Kidney	Caucasioid	Female	54	23/77
	Colon	Caucasoid	Male	75	100/0
	Colon	––	––	––	100/0
	Pancreas	Mongoloid	Male	32	100/0
	Stomach	––	––	––	100/0
	Uterus	––	Female	––	100/0
	Cervix	Caucasoid	Female	59	23/77
	Ovary	Caucasoid	Female	32	100/0
	Prostate	––	Male	––	100/0
Cell (cancer)	HT29[*]	Caucasoid	Female	44	92/8
	A549[*]	Caucasoid	Male	58	96/4
	DLD-1[*]	––	Male	––	25/75
	MCF-7[*]	Caucasoid	Female	69	23/77
	Raji[*]	Neglod	Male	11	17/83
	Panc-1	Caucasoid	Male	56	12/88
	MDA-M-231	Caucasoid	Female	51	100/0
	BT-20	Caucasoid	Female	78	78/22
	T-47D	Caucasoid	Female	54	53/47

[*] Tomitsuka, et al. [59,60].

the difference between type I and type II Fp will bring final conclusion on this attractive idea.

5. Conclusions

The recent findings described in this review indicate that the respiratory chain plays an important role in responses to changes in the amount of oxygen in the environment. Complex II functions as a fumarate reductase during adaptation to a hypoxic condition to ensure the maintenance of oxygen homeostasis. In this connection, the reports indicating that complex II functions as an oxygen sensor are of great interest [63].

In addition, direct evidence of fumarate respiration in human mitochondria are quite important in the study of energy metabolism in hypoxic condition including cancer cells. Differences in energy metabolism between hosts and parasites and/or cancer cells are attractive therapeutic targets.

References

[1] K. Kita, K. Shiomi, S. Ōmura, Parasitology in Japan: advances in drug discovery and biochemical studies, Trends Parasitol. 23 (2007) 223–229.
[2] A. Kroger, V. Geisler, E. Lemma, F. Theis, R. Lenger, Bacterial fumarate respiration, Arch. Microbiol. 158 (1992) 311–314.
[3] T. Kuramochi, H. Hirawake, S. Kojima, S. Takamiya, R. Furushima, T. Aoki, R. Komuniecki, K. Kita, Sequence comparison between the flavoprotein subunit of the fumarate reductase (complex II) of the anaerobic parasitic nematode, Ascaris suum and the succinate dehydrogenase of theaerobic, free-living nematode, Caenorhabditis elegans, Mol. Biochem. Parasitol. 68 (1994) 177–187.
[4] F. Saruta, H. Hirawake, S. Takamiya, Y.-C. Ma, T. Aoki, K. Sekimizu, S. Kojima, K. Kita, Cloning of a cDNA encoding the small subunit of cytochrome b_{558} (cybS) of mitochondrial fumarate reductase (complex II) from adult Ascaris suum, Biochim. Biophys. Acta 1276 (1996) 1–5.
[5] H. Amino, H. Wang, H. Hirawake, F. Saruta, D. Mizuchi, R. Mineki, N. Shindo, K. Murayama, S. Takamiya, T. Aoki, S. Kojima, K. Kita, Stage-specific isoforms of Ascaris suum complex II: the fumarate reductase of the parasitic adult and the succinate dehydrogenase of free-living larvae share a common iron-sulfur subunit, Mol. Biochem. Parasitol. 106 (2000) 63–76.
[6] K. Kita, S. Takamiya, Electron-transfer complexes in Ascaris mitochondria, Adv. Parasitol. 51 (2002) 95–131.
[7] E. Tomitsuka, K. Kita, H. Esumi, Regulation of succinate–ubiquinone reductase and fumarate reductase activities in human complex II by phosphorylation of its flavoprotein subunit, Proc. Jpn. Acad. Ser. B Phys. Biol. Sci. 85 (2009) 258–265.
[8] E. Tomitsuka, K. Kita, H. Esumi, The NADH-fumarate reductase system, a novel mitochondrial energy metabolism, is a new target for anticancer therapy in tumor microenvironments, Ann. N. Y. Acad. Sci. 201 (2011) 44–49.
[9] M.P. Paranagama, K. Sakamoto, H. Amino, M. Awano, H. Miyoshi, K. Kita, Contribution of the FAD and quinone binding sites to the production of reactive oxygen species from Ascaris suum mitochondrial complex II, Mitochondrion 10 (2010) 158–165.
[10] R.D. Guzy, B. Sharma, E. Bell, N.S. Chandel, P.T. Schumacker, Loss of the SdhB, but Not the SdhA, subunit of complex II triggers reactive oxygen species-dependent hypoxia-inducible factor activation and tumorigenesis, Mol. Cell. Biol. 28 (2008) 718–731.
[11] M.A. Selak, S.M. MacKenzie, H. Boulahbel, D.G. Watson, K.D. Mansfield, Y. Pan, M.C. Simon, C.B. Thompson, E. Gottlieb, Succinate links TCA cycle dysfunction to oncogenesis by inhibiting HIF-alpha prolyl hydroxylase, Cancer Cell 7 (2005) 77–85.
[12] R. Komuniecki, B.G. Harris, J. Marr, M. Mueller, Biochemistry and Molecular Biology of Parasites, Academic Press, London, 1995, pp. 49–66.
[13] A.G.M. Tielens, J. Van Hellemond, The electron transport chain in anaerobically functioning eukaryotes, Biochim. Biophys. Acta 1365 (1998) 71–78.
[14] K. Kita, H. Hirawake, S. Takamiya, Cytochromes in the respiratory chain of helminth mitochondria, Int. J. Parasitol. 27 (1997) 617–630.
[15] J. Matsumoto, K. Sakamoto, N. Shinjyo, Y. Kido, N. Yamamoto, K. Yagi, H. Miyoshi, N. Nonaka, K. Katakura, K. Kita, Y. Oku, Anaerobic NADH-fumarate reductase system is predominant in the respiratory chain of Echinococcus multilocularis, providing a novel target for the chemotherapy of alveolar echinococcosis, Antimicrob. Agents Chemother. 52 (2008) 164–170.
[16] P. Kohler, R. Bachmann, Mechanisms of respiration and phosphorylation in Ascaris muscle mitochondria, Mol. Biochem. Parasitol. 1 (1980) 75–90.
[17] H. Oya, K. Kita, in: E. Bennet, C. Behm, C. Bryant (Eds.), Comparative Biochemistry of Parasitic Helminths, Chapman and Hall, London, 1988, pp. 35–53.
[18] S. Takamiya, R. Furushima, R.H. Oya, Electron transfer complexes of Ascaris suum muscle mitochondria: I. Characterization of NADH-cytochrome c reductase (complex I–III), with special reference to cytochrome localization, Mol. Biochem. Parasitol. 13 (1984) 121–134.
[19] S. Takamiya, K. Kita, H. Wang, P.P. Weinstein, A. Hiraishi, H. Oya, T. Aoki Developmental, Changes in the respiratory chain of Ascaris mitochondria, Biochim. Biophys. Acta 1141 (1993) 65–74.
[20] S.T. Cole, C. Condon, B.D. Lemire, J.H. Weiner, Molecular biology, biochemistry and bioenergetics of fumarate reductase, a complex membrane-bound iron-sulfur flavoenzyme of Escherichia coli, Biochim. Biophys. Acta 811 (1985) 381–403.
[21] A. Hiraishi, Fumarate reduction systems in members of the family Rhodospirillaceae with different quinone types, Arch. Microbiol. 150 (1988) 56–60.
[22] F. Iwata, N. Shinjyo, H. Amino, K. Sakamoto, M.K. Islam, N. Tsuji, K. Kita, Change of subunit composition of mitochondrial complex II (succinate–ubiquinone reductase/quinol–fumarate reductase) in Ascaris suum during the migration in the experimental host, Parasitol. Int. 57 (2008) 54–61.

[23] T.M. Iverson, C. Luna-Chavez, G. Cecchini, D.C. Rees, Structure of the *Escherichia coli* fumarate reductase respiratory complex, Science 284 (1999) 1961–1966.

[24] C.R. Lancaster, A. Kröger, M. Auer, H. Michel, Structure of fumarate reductase from *Wolinella succinogenes* at 2.2 A resolution, Nature 402 (1999) 377–385.

[25] K. Kita, C. Vibat, S. Meinhardt, J. Guest, R. Gennis, One-step purification from *Escherichia coli* of complex II (succinate: ubiquinone oxidoreductase) associated with succinate-reducible cytochrome b_{556}, J. Biol. Chem. 264 (1989) 2672–2677.

[26] G. Cecchini, I. Schroder, R.P. Gunsalus, E. Maklashina, Succinate dehydrogenase and fumarate reductase from *Escherichia coli*, Biochim. Biophys. Acta 1553 (2002) 140–157.

[27] C.R.D. Lancaster, Structure and function of succinate: quinone oxidoreductases and the role of quinol: fumarate reductases in fumarate respiration, in: D. Zannoni (Ed.), Respiration in Archaea and Bacteria: Diversity of Prokaryotic Electron Transport Carriers, Kluwer Academic Publishers, The Netherlands, 2004, pp. 57–85.

[28] J.J. Van Hellmond, A. van der Klei, S.W.H. van Weelden, A.G.M. Tielens, Biochemical and evolutionary aspects of anaerobically functioning bacteria, Philos. Trans. R. Soc. B 358 (2003) 205–215.

[29] K. Kita, H. Hirawake, H. Miyadera, H. Amino, S. Takeo, Role of complex II in anaerobic respiration of the parasite mitochondria from *Ascaris suum* and *Plasmodium falciparum*, Biochim. Biophys. Acta 1553 (2002) 123–139.

[30] H.P. Indo, M. Davidson, H.C. Yen, S. Suenaga, K. Tomita, T. Nishii, M. Higuchi, Y. Koga, T. Ozawa, H.J. Majima, Evidence of ROS generation by mitochondria in cells with impaired electron transport chain and mitochondrial DNA damage, Mitochondrion 7 (2007) 106–118.

[31] P. Jezek, L. Hlavata, Mitochondria in homeostasis of reactive oxygen species in cell, tissues, and organism, Int. J. Biochem. Cell Biol. 37 (2005) 2478–2503.

[32] M.P. Murphy, How mitochondria produce reactive oxygen species, Biochem. J. 417 (2009) 1–13.

[33] J. St-Pierre, J.A. Buckingham, S.J. Roebuck, M.D. Brand, Topology of superoxide production from different sites in the mitochondrial electron transport chain, J. Biol. Chem. 277 (2002) 44784–44790.

[34] I.K. Srivastava, H. Rottenberg, A.B. Vaidya, Atovaquone, a broad spectrum antiparasitic drug, collapses mitochondrial membrane potential in a malarial parasite, J. Biol. Chem. 272 (1997) 3961–3966.

[35] S. Looareesuwan, C. Viravan, H.K. Webster, D.E. Kyle, D.B. Hutchinson, C.J. Canﬁeld, Clinical studies of atovaquone, alone or in combination with other antimalarial drugs, for treatment of acute uncomplicated malaria in Thailand, Am. J. Trop. Med. Hyg. 54 (1996) 62–66.

[36] D. Syafruddin, J.E. Siregar, S. Marzuki, Mutations in the cytochrome *b* gene of *Plasmodium berghei* conferring resistance to atovaquone, Mol. Biochem. Parasitol. 104 (1999) 185–194.

[37] I.K. Srivastava, J.M. Morrisey, E. Darrouzet, F. Daldal, A.B. Vaidya, Resistance mutations reveal the atovaquone-binding domain of cytochrome *b* in malaria parasites, Mol. Microbiol. 33 (1999) 704–711.

[38] P. Kohler, R. Bachmann, The effects of the antiparasitic drugs levamisole, thiabendazole, praziquantel, and chloroquine on mitochondrial electron transport in muscle tissue from *Ascaris suum*, Mol. Biochem. Parasitol. 14 (1978) 155–163.

[39] A. Armson, W.B. Grubb, A.H.W. Mendis, The effect of electron transport (ET) inhibitors and thiabendazole on the fumarate reductase (FR) and succinate dehydrogenase (SDH) of *Strongyloides ratti* infective (L3) larvae, Int. J. Parasitol. 25 (1995) 261–263.

[40] S. Omura, H. Miyadera, H. Ui, K. Shiomi, Y. Yamaguchi, R. Masuma, T. Nagamitsu, D. Takano, T. Sunazuka, A. Harder, H. Kölbl, M. Namikoshi, H. Miyoshi, K. Sakamoto, K. Kita, An anthelmintic compound, nafuredin, shows selective inhibition of complex I in helminth mitochondria, Proc. Natl. Acad. Sci. U. S. A. 98 (2001) 60–62.

[41] T. Yamashita, T. Ino, H. Miyoshi, K. Sakamoto, A. Osanai, E. Nakamaru-Ogiso, K. Kita, Rhodoquinone reaction site of mitochondrial complex I, in parasitic helminth, *Ascaris suum*, Mol. Biochem. Parasitol. 100 (2003) 473–477.

[42] H. Miyadera, K. Shiomi, H. Ui, Y. Yamaguchi, R. Masuma, H. Tomoda, H. Miyoshi, A. Osanai, K. Kita, S. Omura, Atpenins, potent and specific inhibitors of mitochondrial complex II (succinate–ubiquinone oxidoreductase), Proc. Natl. Acad. Sci. U. S. A. 100 (2003) 473–477.

[43] A. Osanai, S. Harada, K. Sakamoto, H. Shimizu, D.K. Inaoka, K. Kita, Crystallization of mitochondrial rhodoquinol–fumarate reductase from the parasitic nematode *Ascaris suum* with the specific inhibitor flutolanil, Acta Crystallogr. Sect. F Struct. Biol. Cryst. Commun. 65 (2009) 941–954.

[44] V. Yankovskaya, R. Horsefield, S. Törnroth, C. Luna-Chavez, H. Miyoshi, C. Léger, B. Byrne, G. Cecchini, S. Iwata, Architecture of succinate dehydrogenase and reactive oxygen species generation, Science 299 (2003) 700–704.

[45] F. Sun, X. Huo, Y. Zhai, A. Wang, J. Xu, D. Su, M. Bartlam, Z. Rao, Crystal structure of mitochondrial respiratory membrane protein complex II, Cell 121 (2005) 1043–1057.

[46] L.S. Huang, G. Sun, D. Cobessi, A.C. Wang, J.T. Shen, E.Y. Tung, V.E. Anderson, E.A. Berry, 3-nitropropionic acid is a suicide inhibitor of mitochondrial respiration that, upon oxidation by complex II, forms a covalent adduct with a catalytic base arginine in the active site of the enzyme, J. Biol. Chem. 281 (2006) 5965–5972.

[47] J.P. Bayley, P. Devilee, E.M.P. Taschner, The SDH mutation database: an online resource for succinate dehydrogenase sequence variants involved in pheochromocytoma, paraganglioma and mitochondrial complex II deficiency, BMC Med. Genet. 6 (2005) 39.

[48] B.E. Baysal, On the association of succinate dehydrogenase mutations with hereditary paraganglioma, Trends Endocrinol. Metab. 14 (2003) 453–459.

[49] C. Eng, M. Kiuru, M.J. Fernandez, L.A. Aaltonen, A role for hypoxic mitochondrial enzymes in inherited neoplasia and beyond, Nat. Rev. Cancer 3 (2003) 193–202.

[50] P.J. Pollard, N.C. Wortham, J.P. Tomlinson, The TCA cycle and tumorigenesis: the examples of fumarate hydratase and succinate dehydrogenase, Ann. Med. 35 (2003) 632–639.

[51] P. Rustin, A. Rotig, Inborn errors of complex II–unusual human mitochondrial diseases, Biochim. Biophys. Acta 1553 (2002) 117–122.

[52] N. Ishii, T. Ishii, P.S. Hartman, The role of the electron transport SDHC gene on lifespan and cancer, Mitochondrion 7 (2007) 24–38.

[53] H.X. Hao, O. Khalimonchuk, M. Schraders, N. Dephoure, J.P. Bayley, H. Kunst, P. Devilee, C.W. Cremers, J.D. Schiffman, B.G. Bentz, S.P. Gygi, D.R. Winge, H. Kremer, J. Rutter, SDH5, a gene required for flavination of succinate dehydrogenase, is mutated in paraganglioma, Science 325 (2009) 1139–1142.

[54] M.A. Birch-Machin, R.W. Taylor, B. Cochran, B.A. Ackrell, D.M. Turnbull, Late-onset optic atrophy, ataxia, and myopathy associated with a mutation of a complex II gene, Ann. Neurol. 48 (2000) 330–335.

[55] T. Bourgeron, P. Rustin, D. Chretien, M. Birch-Machin, M. Bourgeois, E. Viegas-Pequignot, A. Munnich, A. Rotig, Mutation of a nuclear succinate dehydrogenase gene results in mitochondrial respiratory chain deficiency, Nat. Genet. 11 (1995) 144–149.

[56] B. Parfait, D. Chretien, A. Rötig, C. Marsac, A. Munnich, P. Rustin, Compound heterozygous mutations in the flavoprotein gene of the respiratory chain complex II in a patient with Leigh syndrome, Hum. Genet. 106 (2000) 236–243.

[57] R. Van Coster, S. Seneca, J. Smet, R. Van Hecke, E. Gerlo, B. Devreese, J. Van Beeumen, J.G. Leroy, L. De Meirleir, W. Lissens, Homozygous Gly555Glu mutation in the nuclear-encoded 70 kDa flavoprotein gene causes instability of the respiratory chain complex II, Am. J. Med. Genet. A 120 (2003) 13–18.

[58] D. Ghezzi, P. Goffrini, G. Uziel, R. Horvath, T. Klopstock, H. Lochmüller, P. D'Adamo, P. Gasparini, T.M. Strom, H. Prokisch, F. Invernizzi, I. Ferrero, M. Zeviani, SDHAF1, encoding a LYR complex-II specific assembly factor, is mutated in SDH-defective infantile leukoencephalopathy, Nat. Genet. 41 (2009) 654–656.

[59] E. Tomitsuka, H. Hirawake, Y. Goto, M. Taniwaki, S. Harada, K. Kita, Direct evidence for two distinct forms of the flavoprotein subunit of human mitochondrial complex II (succinate–ubiquinone reductase), J. Biochem. 134 (2003) 191–195.

[60] E. Tomitsuka, Y. Goto, M. Taniwaki, K. Kita, Direct evidence for expression of type II flavoprotein subunit in human complex II (succinate–ubiquinone reductase), Biochem. Biophys. Res. Commun. 311 (2003) 74–79.

[61] M. Salvi, N. Morrice, A. Brunati, A. Toninello, Identification of the flavoprotein of succinate dehydrogenase and aconitase as in vitro mitochondrial substrates of Fgr tyrosine kinase, FEBS Lett. 581 (2007) 5579–5585.

[62] H. Esumi, J. Lu, Y. Kurashima, T. Hanaoka, Antitumor activity of pyrvinium pamoate, 6-(dimethylamino)-2-[2-(2,5-dimethyl-1-phenyl-1H-pyrrol-3-yl)ethenyl]-1-me thyl-quinolinium pamoate salt, showing preferential cytotoxicity during glucose starvation, Cancer Sci. 95 (2004) 685–690.

[63] B.E. Baysal, R.E. Ferrell, J.E. Willett-Brozick, E.C. Lawrence, D. Myssiorek, A. Bosch, A. van der Mey, P.E. Taschner, W.S. Rubinstein, E.N. Myers, C.W. Richard, C.J. Cornelisse, P. Devilee, B. Devlin, Mutations in SDHD, a mitochondrial complex II gene, in hereditary paraganglioma, Science 287 (2000) 848–851.

[64] J.M. Weinberg, M.A. Venkatachalam, N.F. Roeser, I. Nissim, Mitochondrial dysfunction during hypoxia/reoxygenation and its correction by anaerobic metabolism of citric acid cycle intermediates, Proc. Natl. Acad. Sci. U. S. A. 97 (2000) 2826–2831.

[65] A. Hirayama, K. Kami, M. Sugimoto, M. Sugawara, N. Toki, H. Onozuka, T. Kinoshita, N. Saito, A. Ochiai, M. Tomita, H. Esumi, T. Soga, Quantitative metabolome profiling of colon and stomach cancer microenvironment by capillary electrophoresis time-of-flight mass spectrometry, Cancer Res. 69 (2009) 4918–4925.

Rapid communication

Crystal structure of mitochondrial quinol–fumarate reductase from the parasitic nematode *Ascaris suum*

Hironari Shimizu[1], Arihiro Osanai[1], Kimitoshi Sakamoto[1], Daniel Ken Inaoka[1], Tomoo Shiba[2], Shigeharu Harada[2],* and Kiyoshi Kita[1,†]

[1]Department of Biomedical Chemistry, Graduate School of Medicine, University of Tokyo, 7-3-1 Hongo, Bunkyo-ku, Tokyo 113-0033; and [2]Department of Applied Biology, Graduate School of Science and Technology, Kyoto Institute of Technology, Sakyo-Ku, Kyoto 606-8585, Japan

*Shigeharu Harada, Department of Applied Biology, Graduate School of Science and Technology, Kyoto Institute of Technology, Sakyo-ku, Kyoto 606-8585, Japan. Tel: +81-75-724-7541; Fax: +81-75-724-7541, email: harada@kit.ac.jp

†Kiyoshi Kita, Department of Biomedical Chemistry, Graduate School of Medicine, University of Tokyo, 7-3-1 Hongo, Bunkyo-ku, Tokyo 113-0033, Japan. Tel: +81-3-5841-3526, Fax: +81-3-5841-3444, email: kitak@m.u-tokyo.ac.jp

In the anaerobic respiratory chain of the parasitic nematode *Ascaris suum*, complex II couples the reduction of fumarate to the oxidation of rhodoquinol, a reverse reaction catalyzed by mammalian complex II. In this study, the first structure of anaerobic complex II of mitochondria was determined. The structure, composed of four subunits and five co-factors, is similar to that of aerobic complex II, except for an extra peptide found in the smallest anchor subunit of the *A. suum* enzyme. We discuss herein the structure–function relationship of the enzyme and the critical role of the low redox potential of rhodoquinol in the fumarate reduction of *A. suum* complex II.

Keywords: *Ascaris suum*/crystal structure/mitochondrial respiratory complex II/rhodoquinol–fumarate reductase (QFR)/reaction mechanism.

Abbreviations: $C_{10}M$, *n*-decyl-β-D-maltoside; $C_{12}M$, *n*-dodecyl-β-D-maltoside; C_nE_m, *n*-alkyl ethylene glycol monoether; CybL, cytochrome *b* large subunit of complex II; CybS, cytochrome *b* small subunit of complex II; FAD, flavin adenine dinucleotide; Fp, flavoprotein subunit; Ip, iron–sulphur subunit; NADH, nicotinamide adenine dinucleotide; PEG, polyethyleneglycol; QFR, quinol–fumarate reductase; RQ, rhodoquinone; RQH_2, rhodoquinol; SML, sucrose monolaurate; SQR, succinate–ubiquinone reductase.

The anaerobic respiratory chain, known as the NADH-fumarate reductase (NADH-FRD) system, plays an essential role in the anaerobic energy metabolism of adult *Ascaris suum*, a parasite that inhabits the small intestine, an environment with low oxygen tension (pO_2 of ~4 mmHg). The NADH-FRD system comprises two membrane proteins, complexes I and II, embedded in the mitochondrial inner membrane. Complex I (NADH–rhodoquinone reductase) reduces rhodoquinone (RQ) to rhodoquinol (RQH_2) using the reducing equivalent of NADH, and complex II, which functions as a RQH_2–fumarate reductase (QFR), couples the reduction of fumarate to succinate to the oxidation of RQH_2 to RQ, a reverse reaction catalysed by mammalian complex II (succinate–ubiquinone reductase, SQR) of the aerobic respiratory chain. The anaerobic NADH-fumarate reductase system is found not only in *A. suum* but also in bacteria and many other parasites, and is thus a promising target for chemotherapy (*1-3*).

Although no structure is currently available for eukaryotic QFR-type complex II, structures of SQR-type complex II from porcine (*4*), avian (*5*) and *Escherichia coli* (*6*), as well as those of QFR-type from *E. coli* (*7*) and *Wolinella succinogenes* (*8*), have been determined. Their structures are similar to each other and are generally composed of four polypeptides, the largest flavoprotein subunit (Fp, 70 kDa), an iron–sulphur cluster subunit (Ip, 30 kDa), and cytochrome *b* large (CybL, 15 kDa), and small (CybS, 13 kDa) subunits. In this study, the first X-ray structural analysis of a eukaryotic QFR-type complex II was performed for *A. suum* adult complex II (*A. suum* QFR) in order to clarify the factors responsible for its QFR activity and the mechanisms of RQH_2 oxidation coupled to fumarate reduction.

Ascaris suum QFR was extracted and purified from adult *A. suum* muscle mitochondria and crystallized according to the method described by Osanai *et al.* (*9*). In brief, ~4 kg of *A. suum* obtained from a local slaughterhouse was minced and suspended in Chappell-Perry medium (100 mM KCl, 50 mM Tris–HCl pH 7.4, 5 mM magnesium sulphate, 1 mM ATP, 1 mM EDTA). The fraction containing mitochondria was separated by differential centrifugation, and *A. suum* QFR was then solubilized using 1.0% (w/v) sucrose monolaurate (SML; Dojindo). After purification with anion-exchange column chromatography, SML was exchanged with a mixture of octaethylene glycol monododecyl ether ($C_{12}E_8$) and dodecyl maltoside ($C_{12}M$) by repeated PEG3350 precipitation and dissolution in a buffer containing 0.6% (w/v) $C_{12}E_8$, 0.4% (w/v) $C_{12}M$, 200 mM NaCl, 10 mM Tris–HCl pH 7.5 and 1 mM sodium malonate. Crystallization was performed by the dialysis method using a reservoir solution containing 15% (w/v) PEG3350, 100 mM Tris–HCl pH 8.4, 200 mM NaCl,

1 mM sodium malonate, 0.06% (w/v) $C_{12}E_8$ and 0.04% (w/v) $C_{12}M$. Reddish crystals grew to 100–200 μm in 2–3 days. Crystals of *A. suum* QFR in complex with fumarate were prepared by soaking crystals in the reservoir solution supplemented with 1 mM of sodium fumarate instead of sodium malonate.

X-ray diffraction experiments were performed under a N_2 gas stream (100 K) at SPring-8 beam line BL44XU (Bruker DIP-6040 detector) and at Photon Factory beam line NW12 (ADSC315 CCD detector). Data were processed and scaled using *HKL2000* (*10*). The initial structural model of *A. suum* QFR was solved by molecular replacement using the structure of porcine complex II (pdb code: 1ZOY) as a search model. *Molrep* (*11*) was used for molecular replacement. The refinement of the structure and model building were performed using *Refmac5* (*12*) and *Coot* (*13*), respectively. Data processing and refinement statistics are shown in Supplementary Table SI. All figures were generated using *PyMOL* (*14*). The coordinates have been deposited in the Protein Data Bank under ID codes 3VR8 and 3VRB for the malonate and fumarate bound forms, respectively.

The X-ray structure of *A. suum* QFR (Fig. 1A and B) is composed of Fp, Ip, CybL and CybS subunits, with two molecules in the asymmetric unit (chains A–D and E–H, respectively). As there are no significant differences between the overall protein structures of 3VR8 and 3VRB, we will focus on chains A–D of the malonate-bound form to describe the protein structure as a whole. Fp (chain A) and Ip (chain B) are hydrophilic, whereas CybL (chain C) and CybS (chain D) are hydrophobic membrane-integrated subunits. Fp comprises four domains: a FAD binding

domain (residues A33–A279 and A384–A465), a capping domain (A279–A384), a helical domain (A465–A580) and a C-terminal domain (A580–A645). A FAD prosthetic group is held in the FAD binding domain by a covalent bond to His A79 and by hydrogen bonds with highly conserved residues (Ala A49, Thr A71, Lys A72, Met A73, Ser A78, Thr A80, Gln A84, Gly A85, Gly A86, Ala A201, Asp A255, Glu A421, Arg A432, Ser A437, Leu A438) across amino acid sequences of complex IIs from various species. Ip contains an N-terminal plant ferredoxin-like domain (residues B33–B130) and a C-terminal bacterial ferredoxin-like domain (B130–B281). Of the three iron–sulphur centres bound to Ip, [2Fe–2S] is coordinated by four cysteine residues (B89, B94, B97 and B109) and located in the N-terminal domain, whereas [4Fe–4S] and [3Fe–4S] that are coordinated by four (B182, B185, B188 and B249) and three (B192, B239 and B245) cysteine residues, respectively, are bound to the C-terminal domain. These iron–sulphur centres are also surrounded with highly conserved hydrophobic amino acid residues (Fig. 1C). The structures of Fp and Ip are similar to those of complex IIs with known structures, such as *E. coli* SQR (*6*), *E. coli* QFR (*7*), *W. succinogens* QFR (*8*), porcine SQR (*4*) and avian SQR (*5*).

In contrast to Fp and Ip, the hydrophobic membrane-spanning part shows diversity among species. In *W. succinogens* QFR, it consists of a single polypeptide chain and two haem *b* prosthetic groups, whereas *A. suum* QFR, like *E. coli* SQR, porcine SQR and avian SQR, holds two polypeptide chains (CybL and CybS) and one haem *b*. Both CybL and CybS consist of three membrane-spanning α-helices
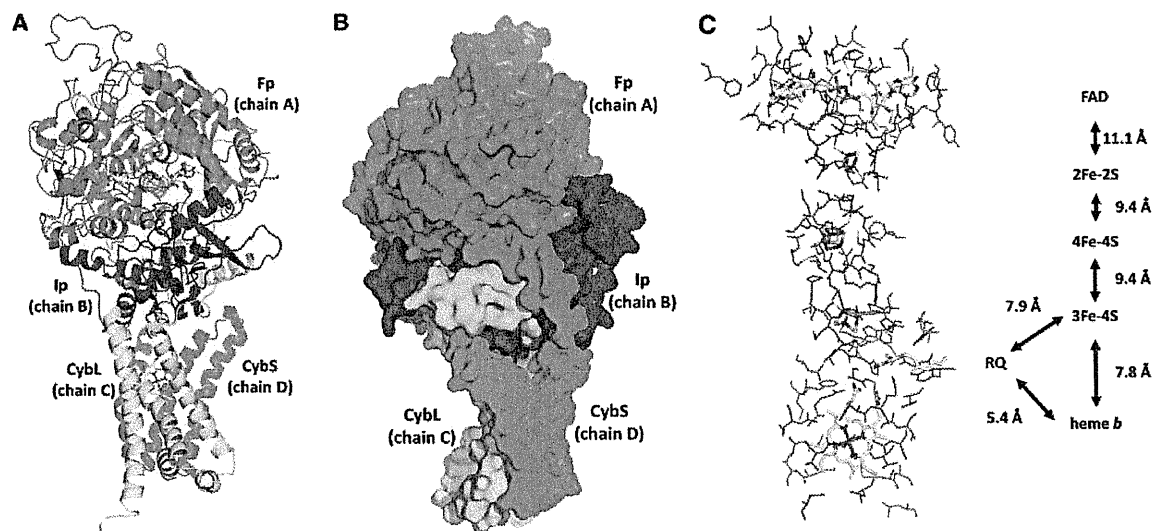
Fig. 1 **Structure of *A. suum* QFR.** Fp (chain A), Ip (chain B), CybL (chain C) and CybS (chain D) are coloured in green, red, yellow and cyan, respectively. Colour code for each atom type: C (yellow), N (blue), O (red), S (orange) and Fe (brown). (A) Cartoon representation of the *A. suum* QFR structure. FAD, iron–sulphur centres and haem *b* are shown as sticks. (B) Surface model of *A. suum* QFR viewed from a different direction from (A) for easy observation of the extra polypeptide attached to the N-terminus of CybS. (C) The arrangement of FAD, [2Fe–2S], [4Fe–4S], [3Fe–4S], haem *b* and RQ. Their edge-to-edge distances are also shown. Amino acid residues within 5 Å of the prosthetic groups and RQ are shown by a wire model. Conserved residues across amino acid sequences of complex IIs are coloured in magenta.

(Fig. 1A and B) and anchor the *A. suum* QFR to the membrane. A haem *b* is embedded into the interface between the CybL and CybS, and two conserved His residues (His C131 and His D95) are ligated to the haem iron. A distinct cleft, whose location is in agreement with the quinone binding sites proposed for other complex IIs, is formed by Ip, CybL and CybS, and a residual electron density probably revealing a bound RQ is detected in the cleft.

Figure 1C shows the arrangement of the prosthetic groups bound to *A. suum* QFR and their edge-to-edge distances. [2Fe–2S], [4Fe–4S] and [3Fe–4S] line between FAD and RQ as observed in other complex IIs (*15*). Thus, the disposition of the prosthetic groups is critical to allow electron transfer from RQH_2 to FAD via the iron–sulphur centres. The hydrophobic environment around the iron–sulphur centres and distances between neighbouring centres (<14 Å) suggest that the electron transfer from RQH_2 to FAD is carried out by quantum tunneling (*16*), as proposed for *E. coli* SQR (*6*).

Figure 2A shows that fumarate is bound near the FAD isoalloxazine ring in a non-planar conformation. C2, C3 and C4 carboxyl group are in the same plane parallel to the isoalloxazine ring, whereas the C1 carboxyl group is twisted around the C1 and C2 bond with a C3–C2–C1–O1A dihedral angle of 83.7°. The twisting, which is stabilized by hydrogen bonds with Gly A85, Thr A288, Glu A289 and Arg A320, suggests that the uniform distribution of π-electrons over the conjugated double bonds of fumarate is broken and a partial charge separation, $C2^{\delta+}$ and $C3^{\delta-}$, is induced. The contact of $C2^{\delta+}$ with FAD N5 (4.05 Å) suggests that a hydride (or hydride equivalent) is transferred from reduced FAD N5 to $C2^{\delta+}$ in the reduction of fumarate with the reduced FAD. Arg A320 is a probable candidate that supplies a proton to $C3^{\delta-}$ to complete the reduction of fumarate. The twisted conformation of fumarate is also observed in flavoproteins with fumarate reductase acitivity (1D4E, 1P2E, 1QLB and 2E6D), and a similar mechanism is proposed for *E. coli* QFR (*17*) and *Trypanosoma cruzi* dihydroorotate dehydrogenase (*18*).

Figure 2B shows the structure of the RQ binding site proposed for *A. suum* QFR. The site is formed by Ip, CybL and CybS, and is in agreement with ubiquinone binding sites suggested for other complex IIs. [3Fe–4S] is the nearest iron–sulphur centre to RQ (9.2 and 7.9 Å from RQ O1 and RQ O2, respectively), suggesting that electrons are first accepted by [3Fe–4S] upon the oxidization of RQH_2, and then transferred to FAD via [4Fe–4S] and [2Fe–2S].

RQ is surrounded by conserved amino acid residues (Ser C72, Arg C76, Asp D106 and Tyr D107) and is involved in hydrogen bond networks, RQ O1–Tyr D107–Arg C76–Asp D106 and RQ O2–Ser C72–RQ N–Arg C76–Asp D106. Protons abstracted from RQH_2 may leave along these networks. It should be noted that the amino group of RQ, which is replaced by the methoxy group in ubiquinone, is involved in one of the hydrogen bond networks.

In this study, the structure of *A. suum* QFR, the first structure of a mitochondrial QFR-type complex II, has
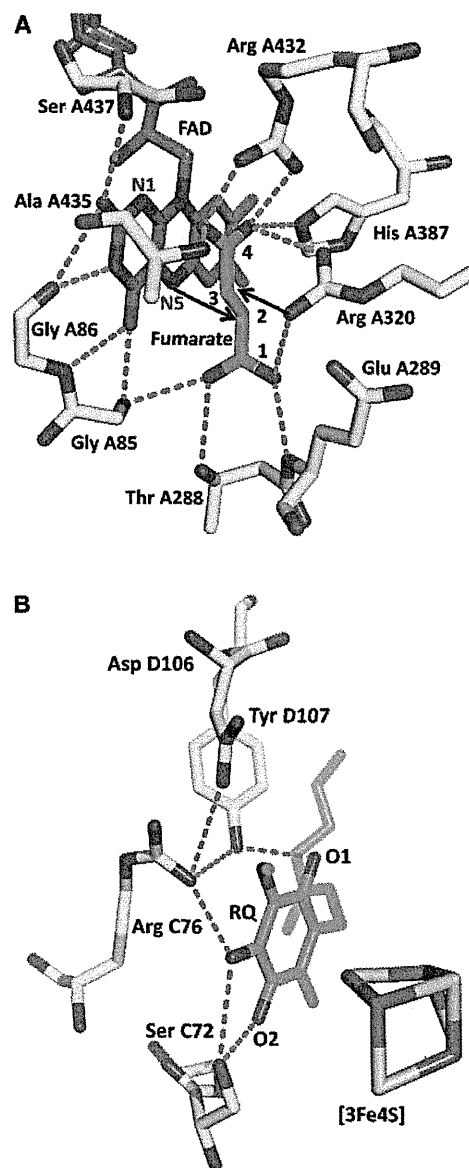

Fig. 2 Close-up views of active site structures of *A. suum* QFR.
(A) Fumarate binding site of *A. suum* QFR. The C1 carboxyl group is twisted around the C1 and C2 bond by hydrogen bonds with nearby residues, which induces partial charge separation, $C2^{\delta+}$ and $C3^{\delta-}$. (B) RQH_2 binding site of *A. suum* QFR. Colour code for each atom type: C (yellow), N (blue), O (red), S (orange) and Fe (brown). Fumarate and RQ are coloured in green, FAD in pink. Hydrogen bonds are drawn with cyan dotted lines.

been determined. A comparison of structures of *A. suum* QFR and SQR-type complex II reveals that not only are the protein structures essentially identical to each other, but also the bound prosthetic groups are surrounded by conserved residues (Fig. 1C). Thus, it appears that the bound quinone type plays a role in determining the direction of catalysis, QFR or SQR of complex II. In fact, *A. suum* QFR, which catalyses the reduction of fumarate ($Em' = +30\,mV$) by oxidizing RQH_2 ($Em' = -63\,mV$) *in vivo*, displays SQR activity,

591

– 404 –

oxidation of succinate ($Em' = +30$ mV), and reduction of ubiquinol ($Em' = +110$ mV) *in vitro*.

The structure also demonstrates a feature unique to *A. suum* QFR. The additional polypeptide composed of 27 residues, which is found only at the N-terminus of *A. suum* CybS, extends to and forms hydrogen bonds with CybL, Ip and Fp (Fig. 1B, cyan), indicating that this unique region probably contributes to the stabilization of the *A. suum* QFR structure. In addition, because no such region has been found in SQR-type complex IIs known to date, this unique feature could make *A. suum* QFR favourable for accepting RQH_2 and fumarate as substrates, although further biochemical and biophysical analyses are necessary to reveal the truth.

Supplementary Data

Supplementary Data are available at *JB* Online.

Conflict of interest
None declared.

References

1. Omura, S., Miyadera, H., Ui, H., Shiomi, K., Yamaguchi, Y., Masuma, R., Nagamitsu, T., Takano, D., Sunazuka, T., Harder, A., Kolbl, H., Namikoshi, M., Miyoshi, H., Sakamoto, K., and Kita, K. (2001) An anthelmintic compound, nafuredin, shows selective inhibition of complex I in helminth mitochondria. *Proc. Natl. Acad. Sci. USA* **98**, 60–62

2. Matsumoto, J., Sakamoto, K., Shinjyo, N., Kido, Y., Yamamoto, N., Yagi, K., Miyoshi, H., Nonaka, N., Katakura, K., Kita, K., and Oku, Y. (2008) Anaerobic NADH-fumarate reductase system is predominant in the respiratory chain of *Echinococcus multilocularis*, providing a novel target for the chemotherapy of alveolar echinococcosis. *Antimicrob. Agents Chemother.* **52**, 164–170

3. Sakai, C., Tomitsuka, E., Esumi, H., Harada, S., and Kita, K. (2012) Mitochondrial fumarate reductase as a target of chemotherapy: from parasites to cancer cells. *Biochim. Biophys. Acta* **1820**, 643–651

4. Sun, F., Huo, X., Zhai, Y., Wang, A., Xu, J., Su, D., Bartlam, M., and Rao, Z. (2005) Crystal structure of mitochondrial respiratory membrane protein complex II. *Cell* **121**, 1043–1057

5. Huang, L.S., Sun, G., Cobessi, D., Wang, A.C., Shen, J.T., Tung, E.Y., Anderson, V.E., and Berry, E.A. (2006) 3-Nitropropionic acid is a suicide inhibitor of

6. Yankovskaya, V., Horsefield, R., Tornroth, S., Luna-Chavez, C., Miyoshi, H., Leger, C., Byrne, B., Cecchini, G., and Iwata, S. (2003) Architecture of succinate dehydrogenase and reactive oxygen species generation. *Science* **299**, 700–704

7. Iverson, T.M., Luna-Chavez, C., Cecchini, G., and Rees, D.C. (1999) Structure of the *Escherichia coli* fumarate reductase respiratory complex. *Science* **284**, 1961–1966

8. Lancaster, C.R., Kroger, A., Auer, M., and Michel, H. (1999) Structure of fumarate reductase from *Wolinella succinogenes* at 2.2 Å resolution. *Nature* **402**, 377–385

9. Osanai, A., Harada, S., Sakamoto, K., Shimizu, H., Inaoka, D.K., and Kita, K. (2009) Crystallization of mitochondrial rhodoquinol-fumarate reductase from the parasitic nematode *Ascaris suum* with the specific inhibitor flutolanil. *Acta Crystallogr. Sect. F Struct. Biol. Cryst. Commun.* **65**, 941–944

10. Otwinowski, Z. and Minor, W. (1997) Macromolecular crystallography part A [20] Processing of X-ray diffraction data collected in oscillation mode. *Methods Enzymol.* **276**, 307–326

11. Vagin, A. and Teplyakov, A. (2010) Molecular replacement with MOLREP. *Acta Crystallogr. D Biol. Crystallogr.* **66**, 22–25

12. Murshudov, G.N., Vagin, A.A., and Dodson, E.J. (1997) Refinement of macromolecular structures by the maximum-likelihood method. *Acta Crystallogr. D Biol. Crystallogr.* **53**, 240–255

13. Emsley, P. and Cowtan, K. (2004) Coot: model-building tools for molecular graphics. *Acta Crystallogr. D Biol. Crystallogr.* **60**, 2126–2132

14. DeLano, W.L. (2002) *The PyMOL Molecular Graphics System*. DeLano Scientific LLC, Palo Alto, California, USA

15. Horsefield, R., Iwata, S., and Byrne, B. (2004) Complex II from a structural perspective. *Curr. Protein Pept. Sci.* **5**, 107–118

16. Page, C.C., Moser, C.C., Chen, X., and Dutton, P.L. (1999) Natural engineering principles of electron tunnelling in biological oxidation-reduction. *Nature* **402**, 47–52

17. Tomasiak, T.M., Archuleta, T.L., Andrell, J., Luna-Chavez, C., Davis, T.A., Sarwar, M., Ham, A.J., McDonald, W.H., Yankovskaya, V., Stern, H.A., Johnston, J.N., Maklashina, E., Cecchini, G., and Iverson, T.M. (2011) Geometric restraint drives on- and off-pathway catalysis by the *Escherichia coli* menaquinol:fumarate reductase. *J. Biol. Chem.* **286**, 3047–3056

18. Inaoka, D.K., Sakamoto, K., Shimizu, H., Shiba, T., Kurisu, G., Nara, T., Aoki, T., Kita, K., and Harada, S. (2008) Structures of *Trypanosoma cruzi* dihydroorotate dehydrogenase complexed with substrates and products: atomic resolution insights into mechanisms of dihydroorotate oxidation and fumarate reduction. *Biochemistry* **47**, 10881–10891

mitochondrial respiration that, upon oxidation by complex II, forms a covalent adduct with a catalytic base arginine in the active site of the enzyme. J. Biol. Chem. 281, 5965–5972
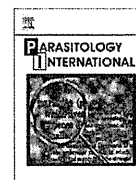
Short communication

Toward understanding the role of mitochondrial complex II in the intraerythrocytic stages of *Plasmodium falciparum*: Gene targeting of the Fp subunit

Takeshi Q. Tanaka [a,1], Makoto Hirai [b], Yoh-ichi Watanabe [a,*], Kiyoshi Kita [a,*]

[a] Department of Biomedical Chemistry, Graduate School of Medicine, The University of Tokyo, 7-3-1 Hongo, Bunkyo-ku, Tokyo 113-0033, Japan
[b] Department of Parasitology, Graduate School of Medicine, Gunma University, 3-39-22 Maebashi City, Gunma 371-8511, Japan

ABSTRACT

Malaria parasites in human hosts depend on glycolysis for most of their energy production, and the mitochondrion of the intraerythrocytic form is acristate. Although the genes for all tricarboxylic acid (TCA) cycle members are found in the parasite genome, the presence of a functional TCA cycle in the intraerythrocytic stage is still controversial. To elucidate the physiological role of *Plasmodium falciparum* mitochondrial complex II (succinate-ubiquinone reductase (SQR) or succinate dehydrogenase (SDH)) in the TCA cycle, the gene for the flavoprotein subunit (Fp) of the enzyme, *pfsdha* (*P. falciparum* gene for SDH subunit A, PlasmoDB ID: PF3D7_1034400) was disrupted. SDH is a well-known marker enzyme for mitochondria. In the *pfsdha* disruptants, Fp mRNA and polypeptides were decreased, and neither SQR nor SDH activity of complex II was detected. The suppression of complex II caused growth retardation of the intraerythrocytic forms, suggesting that complex II contributes to intraerythrocytic parasite growth, although it is not essential for survival. The growth retardation in the *pfsdha* disruptant was rescued by the addition of succinate, but not by fumarate. This indicates that complex II functions as a quinol-fumarate reductase (QFR) to form succinate from fumarate in the intraerythrocytic parasite.

© 2012 Elsevier Ireland Ltd. All rights reserved.

Many aerobic organisms, including humans, depend on oxidative phosphorylation for most of their energy metabolism. On the other hand, the intraerythrocytic malaria parasite synthesizes ATP by anaerobic glycolysis [1]. All the genes for the glycolytic pathway are found in the parasite genome, and pyruvate generated from glucose by glycolysis is converted to lactate with NAD^+ generation [2,3]. The role of mitochondria in parasite energy metabolism is unclear. β-oxidation is absent from the mitochondria and there is no biochemical evidence for a canonical and functional tricarboxylic acid (TCA) cycle in the intraerythrocytic form [2,4,5].

In mammals, mitochondrial complex II functions as a succinate-ubiquinone reductase (SQR) that catalyzes the oxidation of succinate in the TCA cycle and supplies electrons to the respiratory chain. Generally, complex II is composed of four subunits: a flavoprotein subunit (Fp) and an iron–sulfur protein subunit (Ip) as catalytic domains, and two hydrophobic subunits as membrane anchor domains. The genes for the Fp and Ip, *pfsdha* (PlasmoDB ID: PF3D7_1034400) and *pfsdhb*, have been cloned, and *P. falciparum* mitochondrial proteins show both succinate dehydrogenase (SDH) and SQR activities, indicating

that complex II should have some role in parasite survival [6,7]. On the other hand, complex II functions as a quinol-fumarate reductase (QFR), the reverse action of SQR, for anaerobic respiration in various anaerobic organisms [8]. Thus, the direction of the reaction suggests the biological function of complex II.

Since mitochondrial complex II was potentially expected to be essential for parasite survival, a tetracycline analogue-regulated transgene expression system in *P. falciparum* was chosen to establish a conditional knockout strain for the analysis of this potentially essential gene [9]. Since this is a Tet-Off system, the target gene under control is expressed in the absence of the tetracycline analogue anhydrotetracycline (ATc), and the addition of ATc should repress the target gene expression. A conditional knockout of the gene for the Fp subunit in SQR from *P. falciparum* was tried with a pTGPI-GFP derived vector, by which the target gene expression could be controlled with ATc in the parasite (Fig. 1) [9].

As pTGPI-GFP is a 'Tet-Off' system, the transformants were cultured in a medium without ATc, to keep *pfsdha* expression. Stable recombinant parasites had been cloned by limiting dilution from pTSDHA-trunc and pTSDHA-full transformants. The genomic organization of the targeted loci was confirmed by Southern blotting (not shown).

To analyze the *pfsdha* transcription, total RNAs from the trophozoite/schizont-rich culture were used for semi-quantitative RT-PCR and Northern blot analysis. Unexpectedly, the *pfsdha* disruptant did not express *pfsdha* mRNA even in the absence of ATc (not shown). These results indicate that the established *pfsdha* disruptants were not conditional

* Corresponding authors. Tel.: +81 3 5841 3528; fax: +81 3 5841 3444.
E-mail addresses: ywatanab@m.u-tokyo.ac.jp (Y. Watanabe), kitak@m.u-tokyo.ac.jp (K. Kita).
[1] Present address: Laboratory of Malaria and Vector Research, National Institute of Allergy and Infectious Diseases, National Institutes of Health, Rockville, MD 20892, United States.
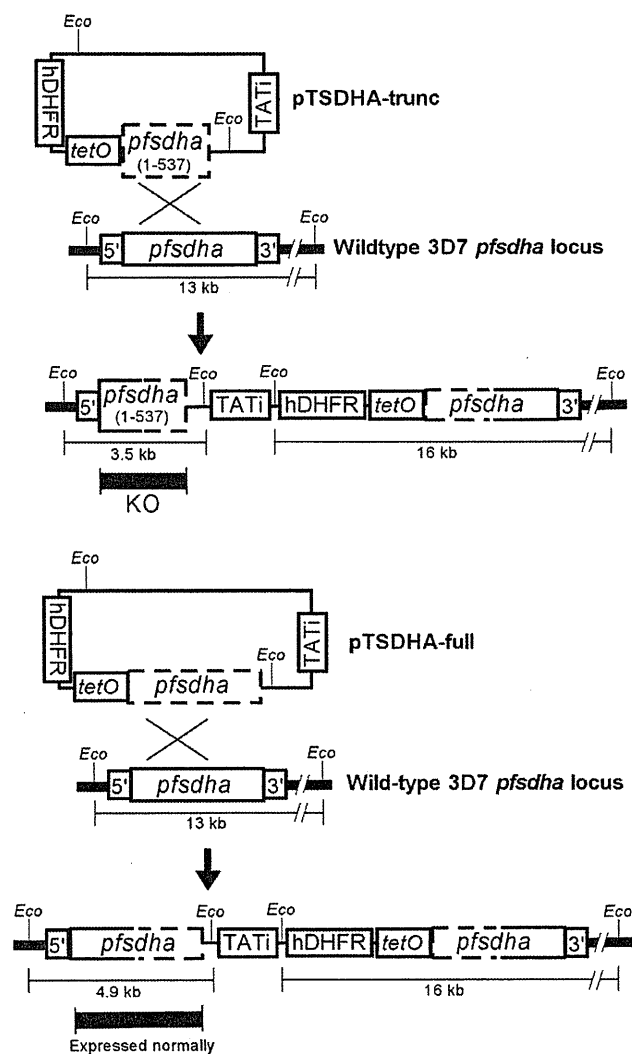
Fig. 1. (A) Schematic diagrams for 'pfsdha disruption' and the control integration into the target locus. The *pfsdha* gene (1–537 and full-length), human dihydrofolate reductase (hDHFR), tetracycline repressor and transactivator fusion protein (TATi3), tetracycline operator sequence (*tetO*), and the EcoRV site (*Eco*) are labeled. Thin and thick solid lines indicate the backbone sequences of the plasmid and the 3D7 chromosomal DNA, respectively. Parasites were cultured following standard protocols [17]. *P. falciparum* (3D7 strain) were cultivated according to [10] with slight modifications. The parental plasmid, pTGPI-GFP, was a kind gift from Dr. B.S. Crabb (Walter and Eliza Hall Institute of Medical Research, Australia) [9]. Since the Rep20 element in pTGPI-GFP is a subtelomeric repeated region and localizes the plasmid to perinuclear chromosome-end clusters [18], and it was expected to potentially inhibit plasmid integration into the homologous chromosomal locus, pTGPI-GFPΔRep20 plasmid was obtained from pTGPI-GFP with BglII digestion and self-ligation. A DNA fragment of *pfsdha* (GenBank ID: XM_001347582, PlasmoDB ID: PF3D7_1034400) corresponding to nucleotide coding region 1–537 with additional sequences of Sse8387I and SpeI sites at each end, allowing for insertion between the PstI and SpeI sites of pTGPI-GFP, was amplified by PCR from 3D7 genomic DNA prepared with DNAzol (Invitrogen, Life Technologies). The PCR product was digested with Sse8387I and SpeI and then inserted into the digested pTGPI-GFPΔRep20, resulting in plasmid pTSDHA-trunc. As a control, a DNA fragment of full-length *pfsdha* with additional sequences of Sse8387I and SpeI sites at each end was amplified by PCR from genomic DNA. The fragment was cloned between the PstI and SpeI sites of pTGPI-GFPΔRep20 by the same method as above, resulting in plasmid pTSDHA-full. The primer sequences were available from the authors upon request. Plasmid DNA was electroporated into infected erythrocytes and transfected parasites were selected with 5 nM WR99210 (Jacobus Pharmaceutical Co., Inc., Princeton, NJ, USA, a kind gift of Dr. David Jacobs) [19]. Single-cell cloning was carried out by limiting dilution.

knockouts, but constitutively *pfsdha*-repressed strains. In a previous study, a similar phenomenon was observed in parasites cultured for prolonged periods (Dr. B.S. Crabb, personal communication). These mutants were useful for the study on the role of complex II in intraerythrocytic form as constitutively *pfsdha*-repressed mutants although the *pfsdha* disruptants were not expected mutants.

Following the analysis of the transcription of *pfsdha* gene, the expression of Fp and Ip peptides was examined by Western blot analysis with mitochondrial proteins prepared from trophozoite/schizont-rich culture [10]. The expression of Fp protein in the mitochondrial fraction from the *pfsdha* disruptant was significantly lower than that of the other controls (not shown). Interestingly, in spite of the normal expression of the *pfsdhb* transcript, repression of Ip protein was observed in the *pfsdha* disruptant (not shown). Although their expressions were not completely repressed, both of the signal intensities for the Fp and Ip proteins of the *pfsdha* disruptant should be low enough to evaluate its role.

The enzyme activities of complex II and dihydroorotate dehydrogenase (DHOD) were examined with mitochondrial proteins isolated from the parasites according to [10]. DHOD is the fourth enzyme of the *de novo* pyrimidine synthetic pathway. *P. falciparum* DHOD localizes on the mitochondrial membrane and transfers electrons to ubiquinone in the respiratory chain [11]. Both SDH and SQR activities in mitochondria from the *pfsdha* disruptant, examined according to [7,10], were repressed to undetectable levels, while mitochondria from the controls showed 3.84 to 6.15 nmol/min/mg of SDH and 3.11 to 5.45 nmol/min/mg of SQR activities. On the other hand, there was no difference in DHOD activities between the controls (13.9 to 18.9 nmol/min/mg) and the *pfsdha* disruptant (15.7 nmol/min/mg).
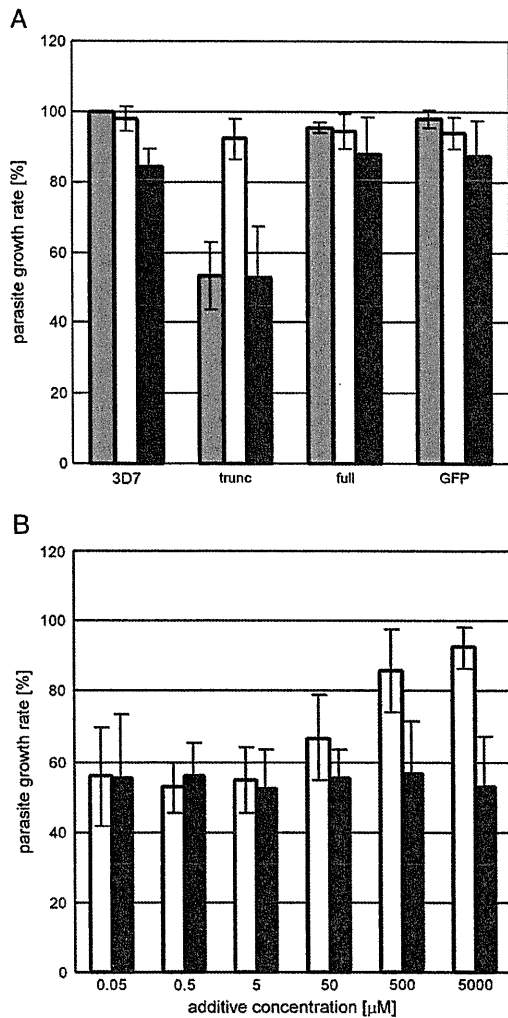
To examine the effect of Fp repression, parasite growth was analyzed after a 48-h culture, one intraerythrocytic growth cycle. As shown in Fig. 2A, the growth retardation was detected in experiments started at 0.2% parasitemia (gray bars). The parasitemia of the controls was $1.78 \pm 0.14\%$ (wild type), $1.73 \pm 0.15\%$ (control of plasmid transfection), and $1.70 \pm 0.15\%$ (control of integration). Meanwhile, the parasitemia of the *pfsdha* disruptant was $0.94\% \pm 0.09\%$, half of that for the controls (Fig. 2A).

Succinate and fumarate are substrates for SQR and QFR, respectively. The direction of the complex II reaction was examined by the addition of the substrates to the *pfsdha* disruptant. The maximum concentration of succinate and fumarate used was 5 mM, because the intraerythrocytic parasite cannot survive in a culture medium with ≥ 50 mM succinate or fumarate (not shown). As a result, 5 mM of succinate rescued the growth retardation of the *pfsdha* disruptant, but fumarate did not (Fig. 2B). The growth of the controls was not affected by the substrate addition. To examine the dose response, the parasites were incubated with between 5 mM and 50 nM of succinate or fumarate. Growth retardation rescue was observed in the *pfsdha* disruptant with ≥ 50 µM of succinate, but fumarate did not rescue the parasite growth retardation (Fig. 2B). These findings suggest that complex II catalyzes succinate production by fumarate reduction in the intraerythrocytic forms.

If the volume of cell and protein concentration [12] is taken account, the concentrations of succinate and fumarate in human cell [13] could be equivalent to those in the parasite (10^{-1} mM) [14]. Thus, under physiological condition, growth retardation of the disruptant in the intraerythrocytic stages may not be observed.

Complex II appears to function as a QFR, and the produced succinate is required in other metabolic pathways. Heme biosynthesis might be a potential pathway that needs the produced succinate, because succinate could be a precursor of succinyl-CoA for the first step of heme biosynthesis. Moreover, QFR has been proposed to couple with protoporphyrinogen IX oxidase in the heme biosynthesis pathway of *P. falciparum* [15]. Our previous observation showing functional link between dihydroorotate-dependent respiration and QRF [7] is consistent with this idea. Considering that a recent report suggested branched TCA cycle metabolism in the parasite [16], further biochemical analysis is indispensable to understand the real nature of the energy metabolism of the parasite.

A

B

We thank Dr. B.S. Crabb and the Walter and Eliza Hall Institute of Medical Research for their kind gift of the pTGPI-GFP vector, and Jacobus Pharmaceuticals for its gift of WR99210. We also thank Prof. K. Tanabe (Osaka University) for his critical advice about the growth experiment of the parasite, Ms. A. Hino (University of Tokyo) for the help in the manuscript preparation, and Dr. Emmanuel O. Balogun (University of Tokyo) for the language correction.

Fig. 2. (A) Growth retardation of the *pfsdha* disruptant and growth rescue by substrates. Gray, white, and black bars indicate no additives, 5 mM of succinate, and 5 mM of fumarate, respectively. (B) Dose dependency of succinate on growth rescue in the *pfsdha* disruptant (pTSDHA-trunc clonal line). White and black bars indicate succinate (Suc) and fumarate (Fum) addition to the *pfsdha* disruptant, respectively. 3D7, wild-type 3D7 strain; trunc, pTSDHA-trunc clonal line ('*pfsdha* disruptant'); full, pTSDHA-full clonal line; GFP, pTGPI-GFPΔRep20 transformant. Synchronized parasites, prepared according to [20], at 0.2% starting parasitemia were triplicated with 1 ml each of complete medium containing 0.5% (w/v) AlbuMAX I (Gibco, Life Technologies). Giemsa-stained smears were prepared after a 48-h incubation without media change, and the parasitemia was evaluated by optical microscopy.

Acknowledgment

References

[1] Roth Jr E. Plasmodium falciparum carbohydrated metabolism: a connection between host cell and parasite. Blood Cells 1990;16:453–60.
[2] Gardner MJ, Hall N, Fung E, White O, Berriman M, Hyman RW, et al. Genome sequence of the human malaria parasite Plasmodium falciparum. Nature 2002;419: 498–511.
[3] Makler MT, Hinrichs DJ. Measurement of the lactate dehydrogenase activity Plasmodium falciparum as an assessment of parasitemia. The American Journal of Tropical Medicine and Hygiene 1993;48:205–10.
[4] Blum JJ, Ginsburg H. Absence of alpha-ketoglutarate dehydrogenase activity and presence of CO_2-fixing activity in Plasmodium falciparum grown in vitro in human erythrocytes. The Journal of Protozoology 1984;31:167–9.
[5] Lang-Unnasch N. Purification and properties of Plasmodium falciparum malate dehydrogenase. Molecular and Biochemical Parasitology 1992;50:17–25.
[6] Takeo S, Kokaze A, Ng CS, Mizuchi D, Watanabe J, Tanabe K, et al. Succinate dehydrogenase in Plasmodium falciparum mitochondria: molecular characterization of the SDHA and SDHB genes for the catalytic subunits, the flavoprotein (Fp) and iron–sulfur (Ip) subunits. Molecular and Biochemical Parasitology 2000;107: 191–205.
[7] Takashima E, Takamiya S, Takeo S, Mi-ichi F, Amino H, Kita K. Isolation of mitochondria from Plasmodium falciparum showing dihydroorotate dependent respiration. Parasitology International 2001;50:273–8.
[8] Sakai C, Tomitsuka E, Esumi H, Harada S, Kita K. Mitochondrial fumarate reductase as a target of chemotherapy: from parasites to cancer cells. Biochimica et Biophysica Acta 2012;1820:643–51.
[9] Meissner M, Krejany E, Gilson PR, de Koning-Ward TF, Soldati D, Crabb BS. Tetracycline analogue-regulated transgene expression in Plasmodium falciparum blood stages using Toxoplasma gondii transactivators. Proceedings of the National Academy of Sciences of the United States of America 2005;102:2980–5.
[10] Kobayashi T, Sato S, Takamiya S, Komaki-Yasuda K, Yano K, Hirata A, et al. Mitochondria and apicoplast of Plasmodium falciparum: behaviour on subcellular fractionation and the implication. Mitochondrion 2007;7:125–32.
[11] Krungkrai J. Purification, characterization and localization of mitochondrial dihydroorotate dehydrogenase in Plasmodium falciparum, human malaria parasite. Biochimica et Biophysica Acta 1995;1243:351–60.
[12] Valverde D, Quintero MR, Candiota AP, Badiella L, Cabañas ME, Arús C. Analysis of the changes in the ^{1}H NMR spectral pattern of perchloric acid extracts of C6 cells with growth. NMR in Biomedicine 2006;19:223–30.
[13] Pollard PJ, Brière JJ, Alam NA, Barwell J, Barclay E, Wortham NC, et al. Accumulation of Krebs cycle intermediates and over-expression of HIF1α in tumours which result from germline FH and SDH mutations. Human Molecular Genetics 2005;14:2231–9.
[14] Teng R, Junankar PR, Bubb WA, Rae C, Mercier P, Kirk K. Metabolite profiling of the intraerythrocytic malaria parasite Plasmodium falciparum by ^{1}H NMR spectroscopy. NMR in Biomedicine 2009;22:292–302.
[15] Nagaraj VA, Arumugam R, Prasad D, Rangarajan PN, Padmanaban G. Protoporphyrinogen IX oxidase from Plasmodium falciparum is anaerobic and is localized to the mitochondrion. Molecular and Biochemical Parasitology 2010;174: 44–52.
[16] Olszewski KL, Mather MW, Morrisey JM, Garcia BA, Vaidya AB, Rabinowitz JD, et al. Branched tricarboxylic acid metabolism in Plasmodium falciparum. Nature 2010;466:774–8.
Erratum in:Nature 2010;469:432.
[17] Trager W, Jensen JB. Human malaria parasites in continuous culture. Science 2004;193:673–5.
[18] O'Donnell RA, Freitas-Junior LH, Preiser PR, Williamson DH, Duraisingh M, McElwain TF, et al. A genetic screen for improved plasmid segregation reveals a role for Rep20 in the interaction of Plasmodium falciparum chromosomes. The EMBO Journal 2002;21:1231–9.
[19] Wu Y, Sifri CD, Lei HH, Su XZ, Wellems TE. Transfection of Plasmodium falciparum within human red blood cells. Proceedings of the National Academy of Sciences of the United States of America 1995;92:973–7.
[20] Lambros C, Vanderberg JP. Synchronization of Plasmodium falciparum erythrocytic stages in culture. The Journal of Parasitology 1979;65:418–20.

Autophagy-Related Atg8 Localizes to the Apicoplast of the Human Malaria Parasite *Plasmodium falciparum*

Kei Kitamura[1,2], Chieko Kishi-Itakura[1], Takafumi Tsuboi[3], Shigeharu Sato[4], Kiyoshi Kita[5], Nobuo Ohta[2]*, Noboru Mizushima[1]*

1 Department of Physiology and Cell Biology, Tokyo Medical and Dental University, Tokyo, Japan, 2 Department of Environmental Parasitology, Tokyo Medical and Dental University, Tokyo, Japan, 3 Cell-Free Science and Technology Research Center and Venture Business Laboratory, Ehime University, Matsuyama, Ehime, Japan, 4 Division of Parasitology, MRC National Institute for Medical Research, London, United Kingdom, 5 Department of Biomedical Chemistry, Graduate School of Medicine, The University of Tokyo, Tokyo, Japan

Abstract

Autophagy is a membrane-mediated degradation process, which is governed by sequential functions of Atg proteins. Although Atg proteins are highly conserved in eukaryotes, protozoa possess only a partial set of Atg proteins. Nonetheless, almost all protozoa have the complete factors belonging to the Atg8 conjugation system, namely, Atg3, Atg4, Atg7, and Atg8. Here, we report the biochemical properties and subcellular localization of the Atg8 protein of the human malaria parasite *Plasmodium falciparum* (PfAtg8). PfAtg8 is expressed during intra-erythrocytic development and associates with membranes likely as a lipid-conjugated form. Fluorescence microscopy and immunoelectron microscopy show that PfAtg8 localizes to the apicoplast, a four membrane-bound non-photosynthetic plastid. Autophagosome-like structures are not observed in the erythrocytic stages. These data suggest that, although *Plasmodium* parasites have lost most Atg proteins during evolution, they use the Atg8 conjugation system for the unique organelle, the apicoplast.

Introduction

Macroautophagy (simply referred to as autophagy hereafter) is a fundamental cellular process, by which cytoplasmic components including proteins and organelles are delivered to the lysosome (or vacuole in yeasts and plants) for degradation. Autophagy is involved in many cellular functions such as adaptation to starvation, cell differentiation, quality control of proteins and organelles, aging, and degradation of invading microbes [1,2,3,4,5,6]. It is also implicated in human diseases such as cancer, inflammatory diseases, and neurodegeneration. Autophagy involves complex membrane dynamics; a membrane cisterna termed the isolation membrane (or phagophore) elongates on the endoplasmic reticulum (ER) and forms a double membrane-bound autophagosome, which contains cytoplasmic materials. Then, the autophagosome fuses with a lysosome to degrade the enclosed materials. Autophagosome formation is the central event of this process and is governed by autophagy-related (Atg) proteins, which were originally identified in yeast [7,8]. The genetic hierarchy of these Atg proteins has been determined and they are classified into at least six functional groups: the starvation-responsive Atg1 kinase complex (Atg1–Atg13–Atg17–Atg29–Atg31), the multi-membrane spanning protein Atg9, the class III phosphatidylinositol 3 (PtdIns 3)-kinase complex (Atg6–Atg14–Vps15–Vps34), the Atg2–Atg18 complex, the Atg12 – Atg5–Atg16

complex ("–" denotes a covalent attachment), and the Atg8–phosphatidylethanolamine (PE) conjugate (Figure 1A) [8,9,10].

These core Atg proteins are highly conserved in most eukaryotes including fungi, animals, and plants [11]. However, recent genome-wide analyses have revealed that they are only partially present in protozoa [12,13]. It is interesting that their conservation pattern is not random; the members belonging to the Atg8 conjugation systems are highly conserved in almost all protozoans, whereas potential homologs of other Atg proteins are only found sporadically (Figure 1A) [12]. The ubiquitin-like protein Atg8 can be covalently conjugated to PE through a sequential reaction that is mediated by a ubiquitin E1-like enzyme, Atg7, and an E2-like enzyme Atg3 [14]. Atg4 cleaves the C-terminal extension of the proform of Atg8 to expose a glycine residue, to which PE is conjugated. Atg4 also catalyzes deconjugation of the PE moiety from Atg8 – PE to release Atg8 from the membrane after completion of autophagosome formation [15]. Although the precise function of Atg8 and its PE conjugation in autophagy remains unclear, it is suggested that Atg8 – PE is important for membrane tethering and hemifusion [16], determination of the autophagosome size [17], and expansion and closure of the isolation membrane [18,19,20]. The partial conservation of the *ATG* genes in protozoans might imply that the smaller set of Atg proteins is sufficient to constitute the autophagosome in these

1

A

S.cerevisiae	H.sapiens	P.falciparum
Atg1	ULK1/2	-
Atg13	Atg13	-
Atg17	FIP200	-
Atg29	Atg101	
Atg31		
Atg9	Atg9A/B	-
Vps34	Vps34	Vps34 (PFE0765W)
Vps15	Vps15	-
Vps30/Atg6	Beclin 1	-
Atg14	Atg14(L)	-
-	AMBRA1	-
Atg2	Atg2A/B	-
Atg18	WIPI1/2/3/4	Atg18 (PF10_0126)
Atg12	Atg12	Atg12 (PF14_0667a)
Atg7	Atg7	Atg7 (PF11_0271)
Atg10	Atg10	-
Atg5	Atg5	Atg5? (PF14_0283)
Atg16	Atg16L1	-
Atg3	Atg3	Atg3 (PFI0280c)
Atg4	Atg4A/B/C/D	Atg4 (PF14_0171)
Atg7	Atg7	Atg7 (PF11_0271)
Atg8	LC3A/B/B2/C GABARAP/L1/L2/L3	Atg8 (PF10_0193)

B

```
1   MKST--FKSEYFFKRKAESERIADRFKNRIPVICKKAE-KSDIBIDKRKYLVPADLTVCQRVYVIRKRI---------   ScAtg8
1   MPSEKTFKQRRTFQRVEDVRLIREQHBTKIPVIIERYKGEKQLPVIDKTKFLVPDHVNMSELIKIIRRRL---------   HsLC3B
1   MPS---LKIEVSFENRVAETHKIRSKYPNRIPVVCERAN-RSNLPIIEKKKFLVPMNMLVGERKFILHQHINQSAYGSNM   PfAtg8

69  MIPHEKAIIIEVN-DTIBHIAALMSAINQEHKLKDGFLYVIYSGENTFGR                                ScAtg8
72  QINANQAFFLLVIGHSMVSVSTPISEVYESEKDEDGFLYMVYASQETFGMKLSV                             HsLC3B
77  KIFRERTIYLEVN-NIVPKIGILLMQDIYEMYKDEDGYLYMPYSQESCLC                                 PfAtg8
```

Figure 1. Atg protein sets are only partially conserved in *P. falciparum*. (A) List of Atg proteins in *S. cerevisiae, Homo sapiens* and *P. falciparum*. –, no ortholog found. It has been suggested that the mammalian FIP200–Atg101 complex and the yeast Atg17–29–31 complex are functional counterparts (dashed boxed) although they do not show significant sequence similarities. None of these factors seems to be conserved in *P. falciparum*. The tag of locus in the *P. falciparum* genome is indicated in parentheses. (B) Alignment of the full sequences of *S. cerevisiae* Atg8, *H. sapiens* LC3B (one of the Atg8 homologs), and *P. falciparum* Atg8. Identical amino acid residues are indicated with filled boxes.
doi:10.1371/journal.pone.0042977.g001

organisms. Alternatively, these organisms may use the Atg8 system for other purposes.

To date, several functional and morphological analyses of autophagy have been performed in protozoan parasites [13]. *Entamoeba invadens* possesses the Atg8 system, but lacks the Atg12 system. Atg8-positive vacuolar structures are generated in a PtdIns 3-kinase-dependent manner during encystation, but its ultrastructure is unknown [21]. In *Trypanosoma cruzi*, autophagosome-like double-membrane structures are formed in epimastigotes and implicated in differentiation into metacyclic trypomastigotes [22,23]. *Leishmania major* seems to have both Atg8 and Atg12 systems [24], and Atg8-positive punctate structures are observed during metacyclogenesis [25]. Accordingly, Atg4-deficient *L. major* shows a defect in differentiation into metacyclic promastigotes [25]. A more recent study performed in *Toxoplasma gondii* showed that genetic depletion of *TgAtg3*, which encodes an enzyme required for Atg8 – PE conjugation, causes growth inhibition and

mitochondrial anomalies, which may be due to a defect in mitophagy [26].

In contrast, the nature of Atg proteins of the malaria parasite *Plasmodium* spp. remains largely unknown. *Plasmodium*, which belongs to phylum Apicomplexa together with *Toxoplasma*, possesses characteristic organelles such as the apicoplast, rhoptry, microneme, and dense granule. The *Plasmodium* sporozoite is transmitted by mosquito and first infects the hepatocyte which generates a large number of infectious merozoites. The merozoite infects erythrocytes and multiplies by schizogony to generate up to ~32 merozoites. Finally the infected erythrocytes rupture, and newly formed merozoites are released into the blood stream. An electron microscopy study of the rodent malaria parasite *P. berghei* demonstrated the presence of autophagosome-like double-membrane structures, which appeared to eliminate micronemes in liver-stage parasites [13,27]. Furthermore, *P. berghei* Atg8 appears to localize to abundant vesicles organized in a reticular network [27].

Because Atg8 – PE is present on both elongating isolation membranes and complete autophagosomes [28,29], Atg8 and its orthologs have been generally recognized as an autophagosome marker. Thus, in this study, we determined the biochemical properties and subcellular localization of Atg8 in *P. falciparum*, the major cause of human malaria. Contrary to our expectation, we found that *P. falciparum* Atg8 (PfAtg8) was specifically associated with the apicoplast, not autophagosomes, during the erythrocytic stage.

Results

Expression of PfAtg8 increases during the erythrocytic stage

Previously, it was reported that the *P. falciparum* genome has only a partial set of core Atg proteins [12,13]. We systematically searched for the orthologs of Atg proteins in the parasite genome and reached a similar conclusion (Figure 1A). We found genes encoding orthologs of a complete set of the Atg8 conjugation system (Atg3, Atg4, Atg7, and Atg8), although other *Atg* genes are only partially conserved (Figure 1A). Compared with Atg8 of the yeast *Saccharomyces cerevisiae*, PfAtg8 shows approximately 40% identity and 65% similarity and has the exposed C-terminal glycine residue, unlike Atg8 orthologs of other organisms (Figure 1B). *P. falciparum* possesses the class III PtdIns 3-kinase Vps34 [30]. In addition, although similarity is not high, there seem to be potential homologs of Atg5 (Figure S1), Atg12 (Figure S2), and Atg18 (Figure S3). Proteins encoded by *PF13_0116* and *PF14_0294* are partially similar to Atg2 and Vps15, respectively, but it remains unknown whether they are orthologs of Atg2 and Vps15.

To analyze endogenous PfAtg8, we generated two independent rabbit polyclonal antibodies against PfAtg8. Both antibodies specifically reacted with a band at approximately 14 kDa (Figure 2A). This size was close to that of Atg8 proteins of other species [28,29]. We used the anti-PfAtg8 antibody #1 in the following experiments unless otherwise specified. The expression level of PfAtg8 was low during early intra-erythrocytic development, but it increased as the parasite matured and reached the maximal level at the late schizont stage (Figure 2B). This pattern was similar to that of HSP70 serving as a cytosolic loading control, suggesting that the apparent increase of PfAtg8 corresponds to the increasing volume of the intra-erythrocytic parasites.

PfAtg8 is associated with membranes

In other organisms, Atg8 is present in two forms: free Atg8 and the membrane-associated form that conjugates with PE embedded in the lipid bilayer. The PE-conjugated and unconjugated forms of Atg8 can be separated by standard SDS-PAGE and urea-containing SDS-PAGE in mammals [29] and yeast [15], respectively. Although Atg8 gains molecular mass when conjugated to PE, its apparent mobility in SDS-PAGE increases probably because of the highly hydrophobic nature of PE. However, PfAtg8 was detected only as a single band in SDS-PAGE (Figure 2A), and no extra band was identified even in the presence of 6 M urea (data not shown). This suggests that the majority of PfAtg8 is present in either the conjugated or unconjugated form. When PfAtg8 was expressed in mammalian cells, PfAtg8 was also detected as a single band, although the mobility was lower than that of PfAtg8 expressed in parasites (Figure 2C). As it is unlikely that PfAtg8 conjugates with PE in mammalian cells, the band detected in mammalian cells is likely to represent the mobility of the unconjugated form. We therefore speculate that PfAtg8 is present primarily in a PE-conjugated form in *Plasmodium*.

We thus investigated whether or not PfAtg8 is membrane bound. The lysates of asynchronous parasites were fractionated by differential centrifugation. PfAtg8 was mainly collected in a low-speed ($13,000 \times g$) pellet (LSP) fraction (Figure 2D). PfAtg8 in the LSP fraction could be solubilized by treatment with 2% Triton X-100, but not with 2 M urea (Figure 2E). This behavior is characteristic of integral membrane proteins, and Atg8 – PE of other organisms have been known to behave in this manner [15,29]. Thus our data suggest that most PfAtg8 is membrane-associated in intra-erythrocytic *Plasmodium*.

In yeast and mammalian cells, Atg8/LC3 associating with the inner autophagosomal membrane is degraded upon fusion with lysosomes [31]. Chloroquine, a well-known anti-malarial drug, impairs lysosomal acidification, and thereby blocks degradation of LC3 in the lysosome [31]. If PfAtg8 is attached to the autophagosomal membrane in *P. falciparum* as are Atg8 or LC3 in yeasts and mammals, this protein should also be degraded within the lytic organelles such as the food vacuole. Chloroquine may affect this process and therefore we examined its effect on the level of PfAtg8. However, treatment of the parasite growing in erythrocytes with chloroquine did not increase the amount of PfAtg8 (Figure 2F), suggesting that PfAtg8 is not involved in the autophagic process at this stage of the parasite's life cycle.

PfAtg8 localizes to the apicoplast membrane

We next determined the subcellular localization of PfAtg8 by immunofluorescence microscopy. In segmented schizonts, the PfAtg8 signal was detected as a single punctate structure in each merozoite (Figure 3). The size of each punctate structure was approximately 200–400 nm. The fact that every parasite possessed one such structure precluded the possibility that the PfAtg8-positive structure is rapidly turned over in the same way as the autophagosome.

The nature of these PfAtg8-positive structures was further characterized by double staining with organelle markers. PfAtg8 did not colocalize with any markers for the merozoite apical organelles such as the microneme (Figure 3A), rhoptry body (Figure 3B), rhoptry neck (Figure 3C), and dense granule (Figure 3D). By contrast, PfAtg8 colocalized with the apicoplast-localizing green fluorescent protein (ACP-GFP) (some of the parasites displayed only weak ACP-GFP expression) [32,33] (Figure 3 F). We confirmed the colocalization between ACP-GFP and PfAtg8 using the independent anti-PfAtg8 antibody #2 (Figure 3G). All the organelles labeled with the ACP-GFP antibody also reacted with the antibody against the plastid-localizing PfHU (histone-like protein, heat unstable), an endogenous apicoplast marker (Figure 3H) [34]. The PfAtg8-positive structure was observed in close proximity to the mitochondrion, and even appeared to overlap part of the organelle (Figure 3E). This partial overlapping between mitochondria and PfAtg8 is consistent with the fact that the apicoplast and the mitochondrion are juxtaposed, probably maintaining physical contact, in the parasite cell [35,36]. To better dissect the localization of PfAtg8, we looked at the parasites at an earlier stage. Morphology of the apicoplast dramatically changes during development inside erythrocytes [32,37]. At the late trophozoite to early schizont stages, the apicoplast forms a tubular or branched shape. In fact, PfAtg8 localized to the tubular or branched apicoplasts, which were clearly distinct from the mitochondria (Figure 4). Taken together, these data suggest that PfAtg8 localizes to the apicoplast during normal development.

Even though the main localization of PfAtg8 is the apicoplast, PfAtg8 could be present on other structures such as autophagosomes. However, the localization pattern of PfAtg8 was not

– 411 –
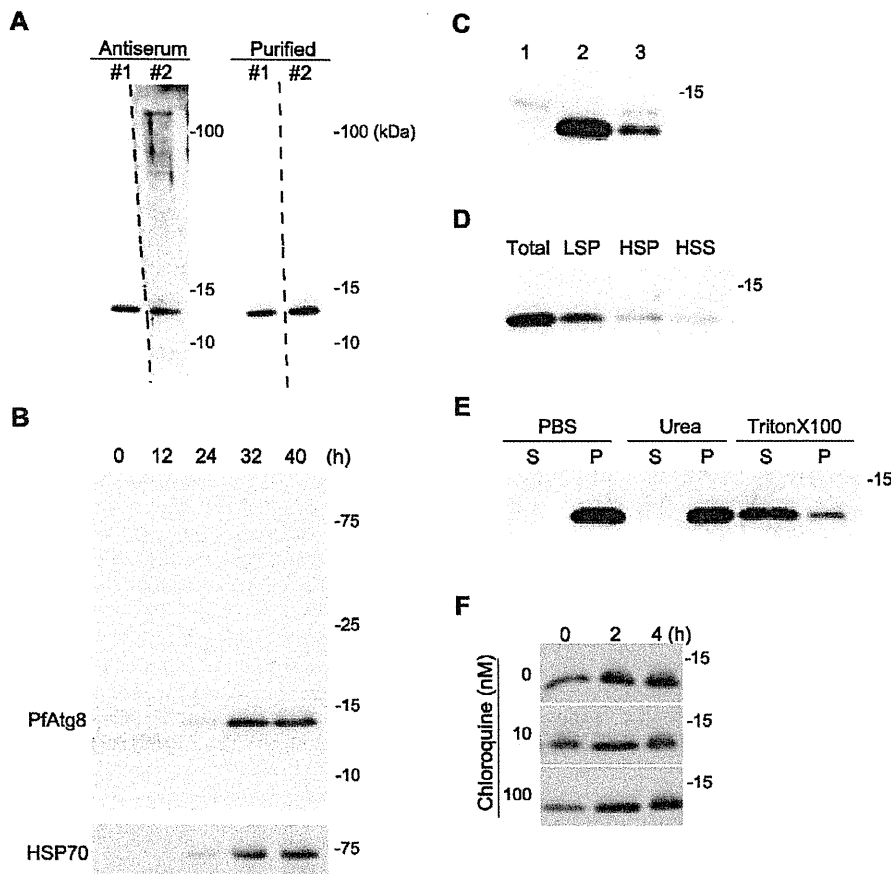
Figure 2. PfAtg8 is associated with membranes. (A) Specificity of the two independently generated anti-PfAtg8 antibodies (#1 and #2). Crude antisera and purified antibodies were used for immunoblotting of lysates of asynchronized *P. falciparum* parasites. (B) Expression of PfAtg8 increases during the erythrocytic stage of development. Highly synchronized *P. falciparum* parasites were collected at 0, 12, 24, 32, and 40 h after invasion. The duration of one cycle of the erythrocyte stage was approximately 42 h. Expression levels of PfAtg8 were analyzed by immunoblotting. An antibody against HSP70 was used as a loading control. (C) PfAtg8 exogenously expressed in mammalian cells (lane 1), endogenous PfAtg8 expressed in *P. falciparum* (lane 2), and the mixture of these two samples were subjected to immunoblot analysis using anti-PfAtg8 antibody. (D) Lysates of asynchronized *Plasmodium* were separated into low-speed (13,000 ×g) pellet (LSP), high-speed (100,000 ×g) pellet (HSP), and high-speed supernatant (HSS) fractions, and analyzed by immunoblotting using anti-PfAtg8 antibody. (E) The LSP fraction prepared in (D) was treated with 2 M urea or 2% Triton-X 100 and separated into 100,000 ×g pellet (P) and supernatant (S). (F) Infected erythrocytes were cultured in the presence of the indicated concentration of chloroquine and expression of PfAtg8 was analyzed.
doi:10.1371/journal.pone.0042977.g002

significantly changed by treatment of chloroquine (Figure 5A), which can typically accumulate autophagosomes/autolysosomes in mammalian cells (as we mentioned above, ACP-GFP was not uniformly expressed and some merozoites displayed only faint GFP signals) [38]. Thus, we could not conclude whether *P. falciparum* can generate PfAtg8-positive autophagosomes. Furthermore, treatment with wortmannin, a PtdIns 3-kinase inhibitor, did not affect PfAtg8 localization, suggesting that association of PfAtg8 with the apicoplast membrane is independent of PtdIns 3-phosphate (Figure 5B).

We further analyzed the localization of PfAtg8 by immunoelectron microscopy using the anti-PfAtg8 antibody. The silver-enhanced gold particles specifically associated with multiple membrane-bound organelles (Figure 6A). The inside of the organelles were filled with relatively low-density materials and a fiber-like structure, which are features of the apicoplast [35,39,40]. These characteristics suggest that the organelles surrounded by PfAtg8 were different from autophagosomes, which are defined as

double membrane-bound organelles containing undigested cyto-plasmic materials, and from autolysosomes, which contain degraded materials [41]. We did not observe such autophagic structures in the parasites in the erythrocytic stage. To confirm that the PfAtg8-positive multi-membrane structures were indeed apicoplasts, we performed immunoelectron microscopy of ACP-GFP-expressing parasites. Anti-GFP antibody specifically reacted with multi-membrane organelles that looked the same as the structures to which PfAtg8 localized (Figure 6A and 6B). The PfAtg8 signals were not detected on the mitochondrion that was in close proximity to the apicoplast (Figure 6A). This suggests that the fluorescence signal detected apparently in the mitochondrion (Figure 3E) was caused by the spatial overlap of the organelle and the apicoplast. Taken together, these data suggest that PfAtg8 specifically localizes to the membrane of the apicoplast in *P. falciparum*.
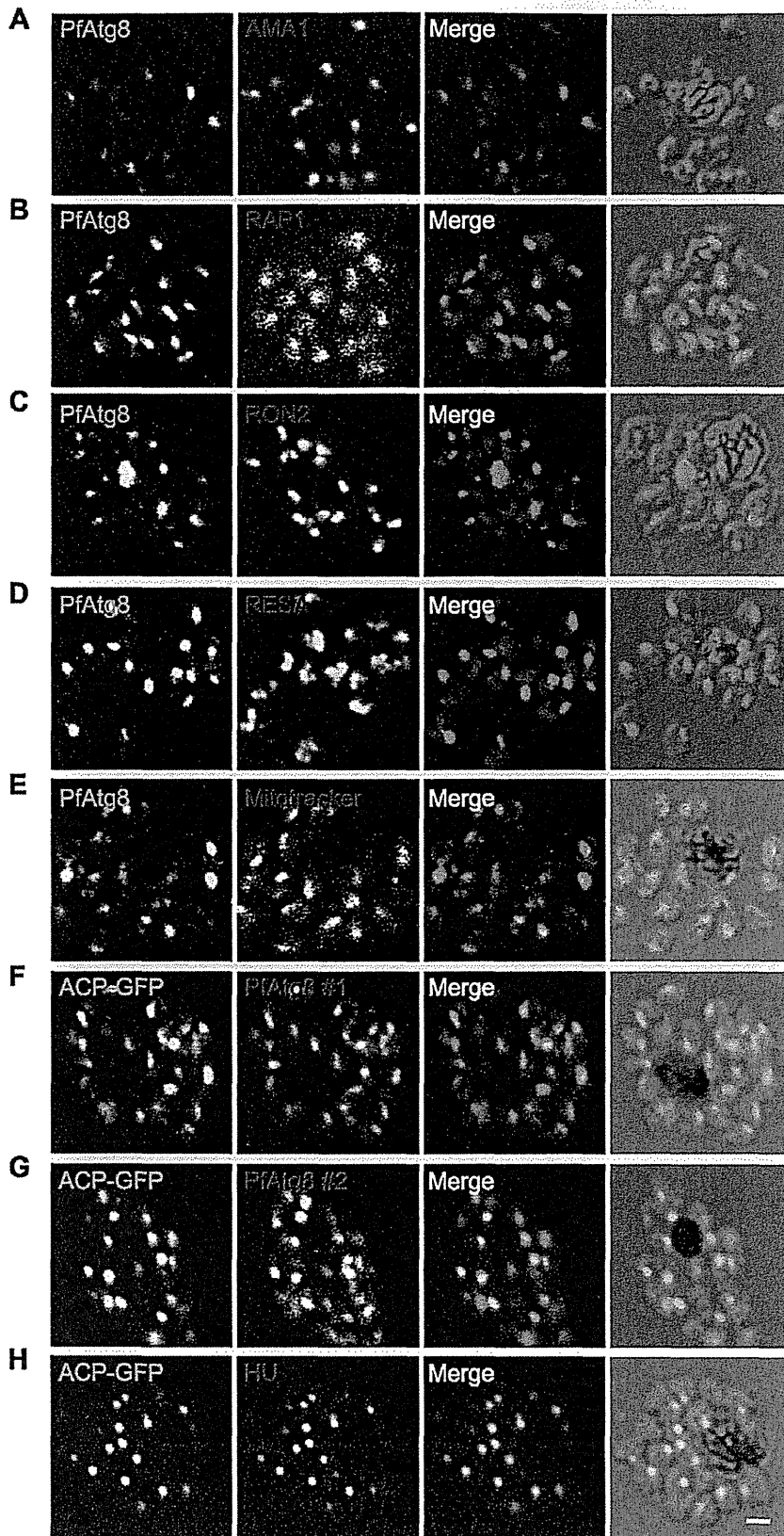
Figure 3. PfAtg8 localizes to the apicoplast. *P. falciparum* FCR3 (A–E) and *P. falciparum* 3D7 transfected with ACP-GFP (F–H) were stained with the indicated organelle markers and visualized by confocal microscopy (because ACP-GFP was not uniformly expressed, some merozoites displayed only faint GFP signals). Anti-PfAtg8 antibody #1 was used in (A–F), and anti-PfAtg8 antibody #2 was used in (G). Apical membrane antigen 1 (AMA1) as a microneme marker (A), rhoptry-associated protein 1 (RAP1) as a rhoptry body marker (B), rhoptry neck protein 2 (RON2) as a rhoptry neck marker (C), the ring-infected erythrocyte surface antigen (RESA) as a dense granule marker (D), MitoTrackerRed CMXRos as a mitochondria marker (E), ACP-GFP (F–H) and the organellar histone-like protein PfHU (H) as an apicoplast marker were used. Scale bar, 1 μm.
doi:10.1371/journal.pone.0042977.g003

Discussion

We report here that PfAtg8 is associated with the apicoplast, probably with the outermost membrane likely in a lipid-conjugated form during the erythrocytic stage. Although we did not detect any autophagosome-like structures in *P. falciparum* even under chloroquine treatment, we do not rule out the possibility that Atg8 can localize to autophagosomes if such structures are formed in *Plasmodium*. The apicoplast is a non-photosynthetic plastid, which is an essential organelle possessing its own genome [40,42,43]. The apicoplast is involved in several metabolic pathways such as biosynthesis of fatty acids, haem, isoprenoid (required for tRNA modification, etc) and iron–sulphur clusters. *P. falciparum* has one plastid, and it physically contacts with the mitochondrion during intraerythrocyte stage [35,36], although the relationship between these two organelles seem to be more complicated in liver stages [44]. The apicoplast has four membranes and that is believed to explain the origin of the organelle from a secondary endosymbiotic alga, most likely a red alga [43,45,46]. The outer two membranes appear to be related to the ER. Nuclear-encoded apicoplast proteins possess an N-terminal signal peptide that is essential for their delivery to the apicoplast via Golgi-independent transport [32,40,47,48,49]. ER-associated protein degradation-like machinery exists in the second outermost membrane [50,51]. Although the autophagosome does not have any ER-related proteins and contribution of other organelles such as mitochondria [52] and the plasma membrane [53], autophagosomes are basically generated on or in close proximity to the ER [8,54]; even direct membrane continuity between the ER and autophagosome has been suggested [55,56]. Therefore, Atg8 may have a shared role in biogenesis of ER-related organelles.

To date, no particular contribution of PfAtg8 on the apicoplast or its biogenesis has been predicted. This protein was suggested to

be essential because deletion of the *Atg8* gene in *P. berghei* causes a lethal phenotype [13,27]. Our ultrastructural analysis, as well as the fact that the parasite has one apicoplast throughout its cell cycle (except for a short period of organellar division), suggest that PfAtg8 is unlikely to be used for autophagic degradation of the apicoplast. Conditional targeting of *Atg3* in *T. gondii* resulted in a severe growth defect with altered mitochondrial morphology [26]. The observed mitochondrial defects might have been caused by a defect in mitochondrial autophagy (mitophagy) as suggested by Besteiro et al., but it may be due to an impaired apicoplast–mitochondria relationship. If the Atg8 conjugation system is involved in essential cellular activities of the malaria parasites, compounds that can inhibit the conjugation reaction (i.e. inhibitors of PfAtg7 or PfAtg3) would be promising therapeutic tools.

P. falciparum contains the class III PtdIns 3-kinase Vps34 (Figure 1A) and PtdIns 3-phosphate is present on both the food vacuole and the apiocoplast membrane [30]. As the Atg8 system functions downstream of the PtdIns 3-kinase complex in starvation-induced autophagy in both yeast and mammals [9,10], we speculated that association between PfAtg8 and the apicoplast membrane could depend on PtdIns 3-kinase activity. However, we observed that treatment of *P. falciparum* with wortmannin did not affect the localization of PfAtg8 (Figure 5B). Recently, it was reported that LC3 (a mammalian Atg8) can associate with membranes even in the absence of upstream Atg factors such as the ULK1/Atg1 complex, Atg9, and PtdIns 3-kinase activity in some types of selective autophagy such as xenophagy against *Salmonella* [57] and Parkin-mediated mitophagy [58]. Nonetheless, the membrane association with LC3 still depends on the two ubiquitin-like LC3 and Atg12 conjugation systems. Therefore, it is possible that the PfAtg8 conjugation system has a unique function, which is independent of most other Atg proteins.
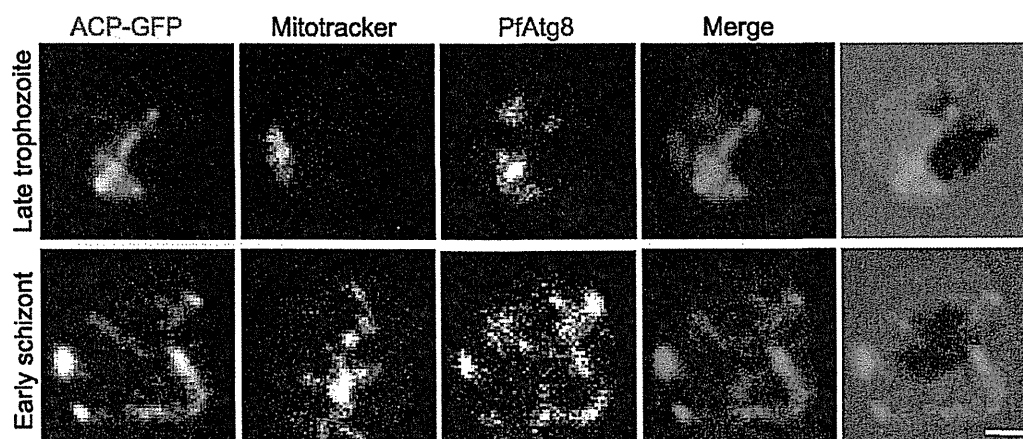

Figure 4. PfAtg8 localizes to tubular and branched apicoplasts. *P. falciparum* transfectant expressing ACP-GFP at late trophozoite and early schizont stages was stained with anti-GFP and anti-PfAtg8 antibodies and MitoTrackerRed CMXRos, and visualized by confocal microscopy. Scale bar, 1 μm.
doi:10.1371/journal.pone.0042977.g004

- 414 -

A

B
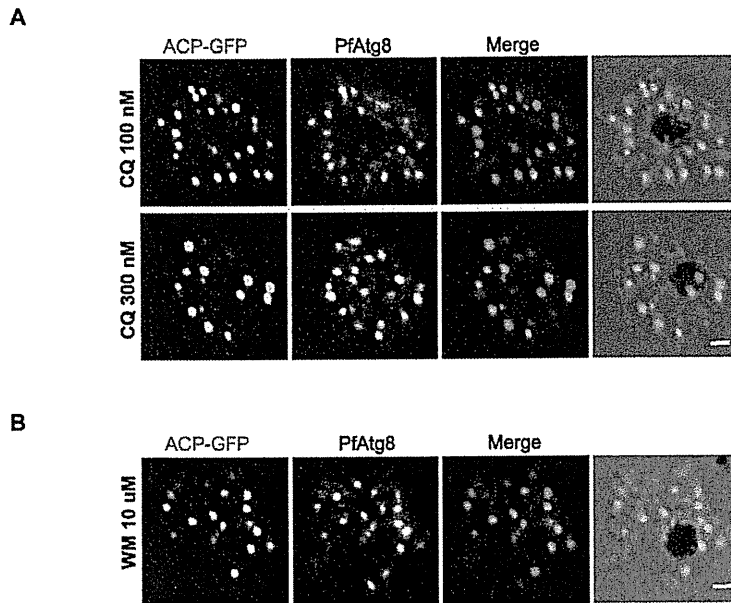
Figure 5. PfAtg8 localization is not affected by chloroquine or wortmannin treatment. *P. falciparum* transfectant expressing ACP-GFP was treated with chloroquine (100 or 300 nM) (A), or wortmannin (10 μM) (B) for 2 h. Scale bar, 1 μm.
doi:10.1371/journal.pone.0042977.g005

Another interesting issue is the requirement of the Atg12 conjugation system. In the autophagy pathway, the Atg8/LC3 conjugation reaction requires an E3-like activity of the Atg12–Atg5 conjugate both in yeast and mammals [59,60]. However,

PfAtg12 lacks the C-terminal glycine residue (Figure S2), which is essential for formation of an isopeptide bond with Atg5. An attractive hypothesis is that PfAtg12 alone may have E3-like activity without Atg5, although the *P. falciparum* genome contains a
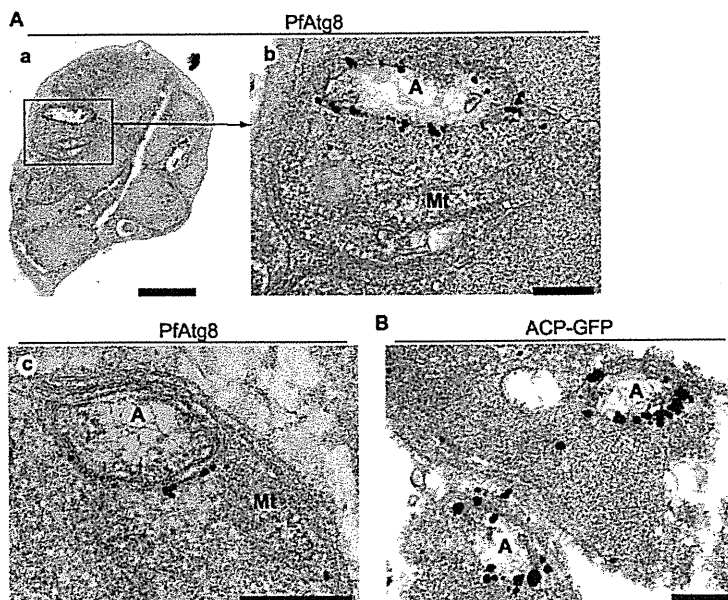
Figure 6. PfAtg8 is associated with the apicoplast membrane. (A) *P. falciparum* FCR3 parasites at the schizont stage were analyzed by immunoelectron microscopy (immunogold and silver enhancement method) with an antibody against PfAtg8 (#1). (a) A schizont in an erythrocyte. (b) A magnified image of the area indicated in (a). (c) Another typical image of a PfAtg8-positive structure. (B) *P. falciparum* transfectant expressing ACP-GFP was analyzed as in panel (A) with an antibody against GFP. A, apicoplast; Mt, mitochondrion. Scale bars, (A, a) 1 μm, (A, b and c, and B) 200 nm.
doi:10.1371/journal.pone.0042977.g006

– 415 –

gene encoding a potential Atg5 homolog (Figure S1). The gene, *PF14_0283* encodes an 863-amino acid (aa) protein that is much larger than yeast (294 aa) and human Atg5 (275 aa). Because of the presence of a number of insertion sequences, it is important to examine whether this Atg5 candidate is a functional Atg5 ortholog that should conjugate and collaborate with PfAtg12 in the organism. Further understanding the roles of Atg8 and Atg12 in *Plasmodium* will provide a general insight into the functions of Atg proteins even in the autophagy pathway.

Materials and Methods

Parasite culture

P. falciparum strain FCR3 was cultured in human B$^+$ erythrocytes as described [61]. In some subcellular localization experiments, the 3D7 parasite strain transfected with pSSPF2/GFP-ACP was used; the transfectant was cultured in the standard culture medium supplemented with 5 nM WR99210 [33]. Where indicated, chloroquine (Sigma-Aldrich) was added to the culture medium. For synchronizing the culture, the red blood cells infected by the late stage schizont were recovered from asynchronous culture by 60% Percoll (GE healthcare) density centrifugation at 2000 ×g for 20 min. After 4 h the culture was treated with 5% D-sorbitol [62], yielding parasites tightly synchronized in the early ring stage (0–4 h after parasite invasion of the erythrocyte).

Cloning of PfAtg8 cDNA and generation of anti-PfAtg8 antibodies

RNA extraction and cDNA synthesis were carried out as described previously [63,64]. GST-fused PfAtg8 recombinant protein was generated using a wheat germ cell-free system [65]. Two independent anti-PfAtg8 antisera (#1 and #2) were raised in two New Zealand white rabbits and the antibodies were purified using GST-PfAtg8 recombinant protein. Animal experimental protocols were approved by the Institutional Animal Care and Use Committee of Tokyo Medical and Dental University (No. 0110115A).

Immunoblotting

Parasites were collected from erythrocytes by treatment with 0.15% saponin (Sigma) in phosphate-buffered saline (PBS) with Complete Protease Inhibitor cocktail (Roche Applied Science), washed three times in PBS and lysed in sample buffer. Parasite extracts were loaded onto 13.5% SDS gel and transferred to a PVDF membrane. Blots were blocked with 5% skim milk in Tris-buffered saline with 0.01% Tween 20 (TBST) and stained with primary antibodies overnight at 4°C. The following primary antibodies were used: rabbit anti-PfAtg8 and mouse monoclonal anti-PfHSP70 antibodies (1:100) [66,67]. After washing with TBST, blots were stained with HRP-conjugated secondary antibodies and visualized with SuperSignal West Pico Chemiluminescent substrate (Thermo Fisher Scientific).

Subcellular fractionation

Asynchronous parasites were harvested as described above. Parasite pellets were disrupted by three cycles of freezing/thawing in MSE buffer (225 mM mannitol, 75 mM sucrose, 0.1 mM EDTA, and 3 mM Tris-HCl [pH 7.4]). Cell debris and intact erythrocytes were removed by centrifugation at 800 ×g for 5 min. The supernatant was spun at 13,000 ×g for 15 min to separate the LSP, and the supernatant was centrifuged again at 100,000 ×g for 60 min to generate the high-speed pellet (HSP) and high-speed supernatant (HSS). The LSP and HSP were resuspended in the same buffer. To analyze solubility, each sample was incubated with 2 M urea or 2% Triton X-100 on ice for 1 h, and then centrifuged at 100,000 ×g for 1 h. The samples were precipitated with ice-cold acetone, resuspended in SDS-PAGE sample buffer, and analyzed by SDS-PAGE.

Expression of PfAtg8 in mammalian cells

PfAtg8 cDNA was inserted into a pCI-neo mammalian expression plasmid (Promega) and transfected into HEK293T cells [68] using Lipofectamine 2000 reagent (Invitrogen). Total cell lysates were subjected to SDS-PAGE and immunoblot analysis.

Immunofluorescence microscopy

Parasite thin blood smears were fixed with 4% paraformaldehyde/PBS for 10 min and samples were permealized with 0.1% Triton X-100/PBS for 15 min. After blocking with 3% bovine serum albumin/PBS for 1 h, samples were incubated with primary and secondary antibodies for 2 h and 1 h, respectively. The smears were mounted with Prolong Gold (Invitrogen). All reactions were carried out at room temperature. Samples were observed with a confocal laser microscope (FV1000D IX81, Olympus) using a 60x PlanApoN oil immersion lens (1.42 NA; Olympus). The following primary antibodies were used: purified rabbit anti-PfAtg8 (1:200 for #1, and 1:100 for #2) antibody, mouse anti-apical membrane antigen (AMA)1 (1:500) [67], anti-rhoptry-associated protein 1 (RAP1, 1:200) [67], anti-rhoptry neck protein 2 (RON2, 1:200) [69], and anti-ring-infected erythrocyte surface antigen (RESA) (23/9, 1:200) [70] antibodies, rabbit anti-PfHU (organellar histone-like protein) antibody [34], and rat anti-GFP antibody (Nacalai Tesque). For visualizing the mitochondrion, parasites were preincubated for 30 min with complete culture medium containing 100 nM MitoTracker Red CMXRos (Molecular Probes).

Immunoelectron microscopy

Mature schizont stage parasites were enriched from synchronous culture using MACS 25LD columns (MiltenyiBiotec) as previously described [71]. For immunoelectron microscopy of *P. falciparum*, the previously described pre-embedding silver enhancement immunogold method [72] was used with slight modifications. The parasitized erythrocytes were fixed in 4% paraformaldehyde and 0.0075% glutaraldehyde dissolved in 0.1 M sodium phosphate buffer (PB) (pH 7.4) for 2 h and then washed three times with PB. Then the cells were permeabilized in liquid nitrogen and incubated in a blocking buffer containing 0.005% saponin, 10% goat serum, 0.1% cold water fish gelatin, and 10% bovine serum albumin for 30 min, and reacted with rabbit anti-PfAtg8 (#1) or rat monoclonal anti-GFP (IgG2a, Nacalai Tesque #04404-84) in blocking buffer at 4°C overnight. Next the cells were washed in PB containing 0.005% saponin and incubated with goat anti-rabbit IgG or anti-rat IgG conjugated with colloidal gold (1.4-nm diameter, Nanogold, Nanoprobes) in blocking buffer for 2 h at room temperature. Cells were washed five times with PB containing 0.005% saponin for 10 min, washed with PB for 5 min, and fixed with 1% glutaraldehyde for 10 min. After washing, the gold partiles were intensified using a silver enhancement kit (HQ silver, Nanoprobes) for 6 min at 20°C in the dark. After washing in distilled water, the cells were post-fixed with 0.03% OsO$_4$ for 15 min at 4°C. After washing with PB, cells were resuspended in 2% gelatin (Sigma) and pelleted again. Microcentrifuge tubes were plunged into ice-cold water to quickly solidify the gelatin with the cells. The tip of the tube was cut open and the cell pellets were retrieved into 15% ethanol, and cut into 1-mm^3 blocks. The blocks were suspended and dehydrated with a graded series of ethanol concentrations, and embedded in epoxy

resin. Ultrathin sections were doubly stained with uranyl acetate and lead citrate and observed using a Hitachi H7100 electron microscope.

Supporting Information

Figure S1 Sequence alignment of Atg5 homologs. Alignment of the sequences of *S. cerevisiae* Atg5, *H. sapiens* Atg5 and *P. falciparum* Atg5. Asterisk (*) shows the position of the Lys residue that receives Atg12 conjugation in yeast and human. This Lys is conserved in PfAtg5.
(TIF)

Figure S2 Sequence alignment of Atg12 homologs. Alignment of the sequences of *S. cerevisiae* Atg12, *H. sapiens* Atg12 and *P. falciparum* Atg12. Asterisk (*) shows the C-terminal Gly residue essential for conjugation with Atg5 in yeast and human. PfAtg12 lacks this Gly residue.
(TIF)

Figure S3 Sequence alignment of Atg18 homologs. Alignment of the sequences of *S. cerevisiae* Atg18, *H. sapiens* WIPI1 and *P. falciparum* Atg18. Asterisk (*) shows the motif required for PtdIns 3-phosphate binding.
(TIF)

Acknowledgments

Author Contributions

Conceived and designed the experiments: K. Kitamura K. Kita NO NM. Performed the experiments: K. Kitamura CK-I TT. Analyzed the data: K. Kitamura CK-I TT SS K. Kita NO NM. Contributed reagents/materials/analysis tools: K. Kitamura TT SS K. Kita NO. Wrote the paper: K. Kitamura CK-I TT SS K. Kita NO NM.

References

1. Cecconi F, Levine B (2008) The role of autophagy in mammalian development: cell makeover rather than cell death. Dev Cell 15: 344–357.
2. Levine B, Kroemer G (2008) Autophagy in the pathogenesis of disease. Cell 132: 27–42.
3. Levine B, Mizushima N, Virgin HW (2011) Autophagy in immunity and inflammation. Nature 469: 323–335.
4. Cuervo AM (2011) Chaperone-mediated autophagy: Dice's 'wild' idea about lysosomal selectivity. Nat Rev Mol Cell Biol 12: 535–541.
5. Rubinsztein DC, Marino G, Kroemer G (2011) Autophagy and aging. Cell 146: 682–695.
6. Mizushima N, Komatsu M (2011) Autophagy: renovation of cells and tissues. Cell 147: 728–741.
7. Nakatogawa H, Suzuki K, Kamada Y, Ohsumi Y (2009) Dynamics and diversity in autophagy mechanisms: lessons from yeast. Nat Rev Mol Cell Biol 10: 458–467.
8. Mizushima N, Yoshimori T, Ohsumi Y (2011) The Role of Atg Proteins in Autophagosome Formation. Annu Rev Cell Dev Biol 27: 107–132.
9. Suzuki K, Kubota Y, Sekito T, Ohsumi Y (2007) Hierarchy of Atg proteins in pre-autophagosomal structure organization. Genes Cells 12: 209–218.
10. Itakura E, Mizushima N (2010) Characterization of autophagosome formation site by a hierarchical analysis of mammalian Atg proteins. Autophagy 6: 764–776.
11. Meijer WH, van der Klei IJ, Veenhuis M, Kiel JAKW (2007) ATG genes involved in non-selective autophagy are conserved from yeast to man, but the selective Cvt and pexophagy pathways also require organism-specific genes. Autophagy 3: 106–116.
12. Rigden DJ, Michels PA, Ginger ML (2009) Autophagy in protists: Examples of secondary loss, lineage-specific innovations, and the conundrum of remodeling a single mitochondrion. Autophagy 5: 784–794.
13. Duszenko M, Ginger ML, Brennand A, Gualdron-Lopez M, Colombo MI, et al. (2011) Autophagy in protists. Autophagy 7: 127–158.
14. Ichimura Y, Kirisako T, Takao T, Satomi Y, Shimonishi Y, et al. (2000) A ubiquitin-like system mediates protein lipidation. Nature 408: 488–492.
15. Kirisako T, Ichimura Y, Okada H, Kabeya Y, Mizushima N, et al. (2000) The reversible modification regulates the membrane-binding state of Apg8/Aut7 essential for autophagy and the cytoplasm to vacuole targeting pathway. J Cell Biol 151: 263–275.
16. Nakatogawa H, Ichimura Y, Ohsumi Y (2007) Atg8, a ubiquitin-like protein required for autophagosome formation, mediates membrane tethering and hemifusion. Cell 130: 165–178.
17. Xie Z, Nair U, Klionsky DJ (2008) Atg8 controls phagophore expansion during autophagosome formation. Mol Biol Cell 19: 3290–3298.
18. Sou YS, Waguri S, Iwata J, Ueno T, Fujimura T, et al. (2008) The Atg8 conjugation system is indispensable for proper development of autophagic isolation membranes in mice. Mol Biol Cell 19: 4762–4775.
19. Fujita N, Hayashi-Nishino M, Fukumoto H, Omori H, Yamamoto A, et al. (2008) An Atg4B mutant hampers the lipidation of LC3 paralogues and causes defects in autophagosome closure. Mol Biol Cell 19: 4651–4659.
20. Weidberg H, Shvets E, Shpilka T, Shimron F, Shinder V, et al. (2010) LC3 and GATE-16/GABARAP subfamilies are both essential yet act differently in autophagosome biogenesis. EMBO J 29: 1792–1802.
21. Picazarri K, Nakada-Tsukui K, Nozaki T (2008) Autophagy during proliferation and encystation in the protozoan parasite *Entamoeba invadens*. Infect Immun 76: 278–288.
22. Alvarez VE, Kosec G, Sant Anna C, Turk V, Cazzulo JJ, et al. (2008) Blocking autophagy to prevent parasite differentiation: a possible new strategy for fighting parasitic infections? Autophagy 4: 361–363.
23. Alvarez VE, Kosec G, Sant'Anna C, Turk V, Cazzulo JJ, et al. (2008) Autophagy is involved in nutritional stress response and differentiation in *Trypanosoma cruzi*. J Biol Chem 283: 3454–3464.
24. Williams RA, Woods KL, Juliano L, Mottram JC, Coombs GH (2009) Characterization of unusual families of ATG8-like proteins and ATG12 in the protozoan parasite *Leishmania major*. Autophagy 5: 159–172.
25. Besteiro S, Williams RA, Morrison LS, Coombs GH, Mottram JC (2006) Endosome sorting and autophagy are essential for differentiation and virulence of *Leishmania major*. J Biol Chem 281: 11384–11396.
26. Besteiro S, Brooks CF, Striepen B, Dubremetz JF (2011) Autophagy Protein Atg3 is Essential for Maintaining Mitochondrial Integrity and for Normal Intracellular Development of *Toxoplasma gondii* Tachyzoites. PLoS Pathog 7: e1002416.
27. Brennand A, Gualdron-Lopez M, Coppens I, Rigden DJ, Ginger ML, et al. (2011) Autophagy in parasitic protists: unique features and drug targets. Mol Biochem Parasitol 177: 83–99.
28. Kirisako T, Baba M, Ishihara N, Miyazawa K, Ohsumi M, et al. (1999) Formation process of autophagosome is traced with Apg8/Aut7p in yeast. J Cell Biol 147: 435–446.
29. Kabeya Y, Mizushima N, Ueno T, Yamamoto A, Kirisako T, et al. (2000) LC3, a mammalian homologue of yeast Apg8p, is localized in autophagosome membranes after processing. EMBO J 19: 5720–5728.
30. Tawk L, Chicanne G, Dubremetz JF, Richard V, Payrastre B, et al. (2010) Phosphatidylinositol 3-phosphate, an essential lipid in *Plasmodium*, localizes to the food vacuole membrane and the apicoplast. Eukaryot Cell 9: 1519–1530.
31. Mizushima N, Yoshimori T, Levine B (2010) Methods in mammalian autophagy research. Cell 140: 313–326.
32. Waller RF, Reed MB, Cowman AF, McFadden GI (2000) Protein trafficking to the plastid of *Plasmodium falciparum* is via the secretory pathway. EMBO J 19: 1794–1802.
33. Sato S, Rangachari K, Wilson RJ (2003) Targeting GFP to the malarial mitochondrion. Mol Biochem Parasitol 130: 155–158.
34. Sasaki N, Hirai M, Maeda K, Yui R, Itoh K, et al. (2009) The *Plasmodium* HU homolog, which binds the plastid DNA sequence-independent manner, is essential for the parasite's survival. FEBS Lett 583: 1446–1450.
35. Hopkins J, Fowler R, Krishna S, Wilson I, Mitchell G, et al. (1999) The plastid in *Plasmodium falciparum* asexual blood stages: a three-dimensional ultrastructural analysis. Protist 150: 283–295.
36. Kobayashi T, Sato S, Takamiya S, Komaki-Yasuda K, Yano K, et al. (2007) Mitochondria and apicoplast of *Plasmodium falciparum*: behaviour on subcellular fractionation and the implication. Mitochondrion 7: 125–132.
37. van Dooren GG, Marti M, Tonkin CJ, Stimmler LM, Cowman AF, et al. (2005) Development of the endoplasmic reticulum, mitochondrion and apicoplast during the asexual life cycle of Plasmodium falciparum. Mol Microbiol 57: 405–419.
38. Chen D, Fan W, Lu Y, Ding X, Chen S, et al. (2012) A mammalian autophagosome maturation mechanism mediated by TECPR1 and the Atg12-Atg5 conjugate. Mol Cell 45: 629–641.
39. McFadden GI, Roos DS (1999) Apicomplexan plastids as drug targets. Trends Microbiol 7: 328–333.
40. McFadden GI (2011) The apicoplast. Protoplasma 248: 641–650.
41. Eskelinen E-L (2005) Maturation of autophagic vacuoles in mammalian cells. Autophagy 1: 1–10.
42. Ralph SA, van Dooren GG, Waller RF, Crawford MJ, Fraunholz MJ, et al. (2004) Tropical infectious diseases: metabolic maps and functions of the *Plasmodium falciparum* apicoplast. Nat Rev Microbiol 2: 203–216.

- 417 -

43. Kalanon M, McFadden GI (2010) Malaria, *Plasmodium falciparum* and its apicoplast. Biochem Soc Trans 38: 775–782.
44. Stanway RR, Mueller N, Zobiak B, Graewe S, Froehlke U, et al. (2011) Organelle segregation into Plasmodium liver stage merozoites. Cell Microbiol 13: 1768–1782.
45. Kohler S, Delwiche CF, Denny PW, Tilney LG, Webster P, et al. (1997) A plastid of probable green algal origin in Apicomplexan parasites. Science 275: 1485–1489.
46. Janouskovec J, Horak A, Obornik M, Lukes J, Keeling PJ (2010) A common red algal origin of the apicomplexan, dinoflagellate, and heterokont plastids. Proc Natl Acad Sci U S A 107: 10949–10954.
47. Tonkin CJ, Struck NS, Mullin KA, Stimmler LM, McFadden GI (2006) Evidence for Golgi-independent transport from the early secretory pathway to the plastid in malaria parasites. Mol Microbiol 61: 614–630.
48. Tonkin CJ, Kalanon M, McFadden GI (2008) Protein targeting to the malaria parasite plastid. Traffic 9: 166–175.
49. Lim L, Kalanon M, McFadden GI (2009) New proteins in the apicoplast membranes: time to rethink apicoplast protein targeting. Trends Parasitol 25: 197–200.
50. Kalanon M, Tonkin CJ, McFadden GI (2009) Characterization of two putative protein translocation components in the apicoplast of *Plasmodium falciparum*. Eukaryot Cell 8: 1146–1154.
51. Spork S, Hiss JA, Mandel K, Sommer M, Kooij TW, et al. (2009) An unusual ERAD-like complex is targeted to the apicoplast of *Plasmodium falciparum*. Eukaryot Cell 8: 1134–1145.
52. Hailey DW, Rambold AS, Satpute-Krishnan P, Mitra K, Sougrat R, et al. (2010) Mitochondria supply membranes for autophagosome biogenesis during starvation. Cell 141: 656–667.
53. Ravikumar B, Moreau K, Jahreiss L, Puri C, Rubinsztein DC (2010) Plasma membrane contributes to the formation of pre-autophagosomal structures. Nat Cell Biol 12: 747–757.
54. Kovács AL, Pálfia Z, Réz G, Vellai T, Kávacs J (2007) Sequestration revisited: integrating traditional electron microscopy, de novo assembly and new results. Autophagy 3: 655–662.
55. Yla-Anttila P, Vihinen H, Jokitalo E, Eskelinen EL (2009) 3D tomography reveals connections between the phagophore and endoplasmic reticulum. Autophagy 5: 1180–1185.
56. Hayashi-Nishino M, Fujita N, Noda T, Yamaguchi A, Yoshimori T, et al. (2009) A subdomain of the endoplasmic reticulum forms a cradle for autophagosome formation. Nat Cell Biol 11: 1433–1437.
57. Kageyama S, Omori H, Saitoh T, Sone T, Guan JL, et al. (2011) The LC3 recruitment mechanism is separate from Atg9L1-dependent membrane formation in the autophagic response against *Salmonella*. Mol Biol Cell.
58. Itakura E, Kishi-Itakura C, Koyama-Honda I, Mizushima N (2012) Structures containing Atg9A and the ULK1 complex independently target depolarized mitochondria at initial stages of Parkin-mediated mitophagy. J Cell Sci 125: 1488–1499.
59. Suzuki K, Kirisako T, Kamada Y, Mizushima N, Noda T, et al. (2001) The pre-autophagosomal structure organized by concerted functions of *APG* genes is essential for autophagosome formation. EMBO J 20: 5971–5981.
60. Mizushima N, Yamamoto A, Hatano M, Kobayashi Y, Kabeya Y, et al. (2001) Dissection of autophagosome formation using Apg5-deficient mouse embryonic stem cells. J Cell Biol 152: 657–667.
61. Trager W, Jensen JB (1976) Human malaria parasites in continuous culture. Science 193: 673–675.
62. Lambros C, Vanderberg JP (1979) Synchronization of *Plasmodium falciparum* erythrocytic stages in culture. J Parasitol 65: 418–420.
63. Kyes S, Pinches R, Newbold C (2000) A simple RNA analysis method shows var and rif multigene family expression patterns in *Plasmodium falciparum*. Mol Biochem Parasitol 105: 311–315.
64. Dzikowski R, Frank M, Deitsch K (2006) Mutually exclusive expression of virulence genes by malaria parasites is regulated independently of antigen production. PLoS Pathog 2: e22.
65. Tsuboi T, Takeo S, Iriko H, Jin L, Tsuchimochi M, et al. (2008) Wheat germ cell-free system-based production of malaria proteins for discovery of novel vaccine candidates. Infect Immun 76: 1702–1708.
66. Tsuji M, Mattei D, Nussenzweig RS, Eichinger D, Zavala F (1994) Demonstration of heat-shock protein 70 in the sporozoite stage of malaria parasites. Parasitol Res 80: 16–21.
67. Ito D, Han ET, Takeo S, Thongkukiatkul A, Otsuki H, et al. (2011) Plasmodial ortholog of *Toxoplasma gondii* rhoptry neck protein 3 is localized to the rhoptry body. Parasitol Int 60: 132–138.
68. DuBridge RB, Tang P, Hsia HC, Leong PM, Miller JH, et al. (1987) Analysis of mutation in human cells by using an Epstein-Barr virus shuttle system. Mol Cell Biol 7: 379–387.
69. Cao J, Kaneko O, Thongkukiatkul A, Tachibana M, Otsuki H, et al. (2009) Rhoptry neck protein RON2 forms a complex with microneme protein AMA1 in *Plasmodium falciparum* merozoites. Parasitol Int 58: 29–35.
70. Culvenor JG, Day KP, Anders RF (1991) *Plasmodium falciparum* ring-infected erythrocyte surface antigen is released from merozoite dense granules after erythrocyte invasion. Infect Immun 59: 1183–1187.
71. Ribaut C, Berry A, Chevalley S, Reybier K, Morlais I, et al. (2008) Concentration and purification by magnetic separation of the erythrocytic stages of all human *Plasmodium* species. Malar J 7: 45.
72. Hayashi M, Taniguchi S, Ishizuka Y, Kim HS, Wataya Y, et al. (2001) A homologue of N-ethylmaleimide-sensitive factor in the malaria parasite *Plasmodium falciparum* is exported and localized in vesicular structures in the cytoplasm of infected erythrocytes in the brefeldin A-sensitive pathway. J Biol Chem 276: 15249–15255.

- 418 -

nature
genetics

Plasmodium cynomolgi genome sequences provide insight into *Plasmodium vivax* and the monkey malaria clade

Shin-Ichiro Tachibana[1,13], Steven A Sullivan[2], Satoru Kawai[3], Shota Nakamura[4], Hyunjae R Kim[2], Naohisa Goto[4], Nobuko Arisue[5], Nirianne M Q Palacpac[5], Hajime Honma[1,5], Masanori Yagi[5], Takahiro Tougan[5], Yuko Katakai[6], Osamu Kaneko[7], Toshihiro Mita[8], Kiyoshi Kita[9], Yasuhiro Yasutomi[10], Patrick L Sutton[2], Rimma Shakhbatyan[2], Toshihiro Horii[5], Teruo Yasunaga[4], John W Barnwell[11], Ananias A Escalante[12], Jane M Carlton[2,14] & Kazuyuki Tanabe[1,5,14]

P. cynomolgi, a malaria-causing parasite of Asian Old World monkeys, is the sister taxon of *P. vivax*, the most prevalent malaria-causing species in humans outside of Africa. Because *P. cynomolgi* shares many phenotypic, biological and genetic characteristics with *P. vivax*, we generated draft genome sequences for three *P. cynomolgi* strains and performed genomic analysis comparing them with the *P. vivax* genome, as well as with the genome of a third previously sequenced simian parasite, *Plasmodium knowlesi*. Here, we show that genomes of the monkey malaria clade can be characterized by copy-number variants (CNVs) in multigene families involved in evasion of the human immune system and invasion of host erythrocytes. We identify genome-wide SNPs, microsatellites and CNVs in the *P. cynomolgi* genome, providing a map of genetic variation that can be used to map parasite traits and study parasite populations. The sequencing of the *P. cynomolgi* genome is a critical step in developing a model system for *P. vivax* research and in countering the neglect of *P. vivax*.

Human malaria is transmitted by anopheline mosquitoes and is caused by four species in the genus *Plasmodium*. Of these, *P. vivax* is the major malaria agent outside of Africa, annually causing 80–100 million cases[1]. Although *P. vivax* infection is often mistakenly regarded as benign and self-limiting, *P. vivax* treatment and control present challenges distinct from those of the more virulent *Plasmodium falciparum*. Biological traits, including a dormant (hypnozoite) liver stage responsible for recurrent infections (relapses), early infective sexual stages (gametocytes) and transmission from low parasite

densities in the blood[2], coupled with emerging antimalarial drug resistance[3], render *P. vivax* resilient to modern control strategies. Recent evidence indicates that *P. falciparum* derives from parasites of great apes in Africa[4], whereas *P. vivax* is more closely related to parasites of Asian Old World monkeys[5–7], although not itself infective of these monkeys.

P. vivax cannot be cultured *in vitro*, and the small New World monkeys capable of hosting it are rare and do not provide an ideal model system. *P. knowlesi*, an Asian Old World monkey parasite recently recognized as a zoonosis for humans[8], has had its genome sequenced[9], but the species is distantly related to *P. vivax* and is phenotypically dissimilar. In contrast, *P. cynomolgi*, a simian parasite that can infect humans experimentally[10], is the closest living relative (a sister taxon) to *P. vivax* and possesses most of the same genetic, phenotypic and biological characteristics—notably, periodic relapses caused by dormant hypnozoites, early infectious gametocyte formation and invasion of Duffy blood group–positive reticulocytes. *P. cynomolgi* thus offers a robust model for *P. vivax* in a readily available laboratory host, the Rhesus monkey, whose genome was recently sequenced[11]. Here, we report draft genome sequences of three *P. cynomolgi* strains and comparative genomic analyses of *P. cynomolgi*, *P. vivax*[12] and *P. knowlesi*[9], three members of the monkey malaria clade.

We sequenced the genome of *P. cynomolgi* strain B, isolated from a monkey in Malaysia and grown in splenectomized monkeys (Online Methods). A combination of Sanger, Roche 454 and Illumina chemistries was employed to generate a high-quality reference assembly at 161-fold coverage, consisting of 14 supercontigs (corresponding to the 14 parasite chromosomes) and ~1,649 unassigned contigs, comprising